U. S. Department
of Transportation
**Federal Railroad
Administration**

Aerodynamic Effects of High-Speed Passenger Trains on Other Trains

Office of Research
and Development
Washington, D.C. 20590

Safety of High-Speed Ground Transportation Systems

DOT/FRA/ORD-01/12

**Final Report
April 2002**

REPORT DOCUMENTATION PAGE

Form Approved
OMB No. 0704-0188

1. AGENCY USE ONLY (Leave blank)	2. REPORT DATE	3. REPORT TYPE AND DATES COVERED
	April 2002	Final Report September 2000-March 2001

4. TITLE AND SUBTITLE
Aerodynamic Effects of High-Speed Passenger Trains on Other Trains

5. FUNDING NUMBERS
RR193/R1061

6. AUTHOR(S)
Samuel Holmes and Martin P. Schroeder

7. PERFORMING ORGANIZATION NAME(S) AND ADDRESS(ES)
Applied Research Associates, Inc.*
4300 San Mateo Blvd. NE, Suite A-220
Albuquerque, New Mexico 87110

8. PERFORMING ORGANIZATION REPORT NUMBER
DOT-VNTSC-FRA-01-05

9. SPONSORING/MONITORING AGENCY NAME(S) AND ADDRESS(ES)
U.S. Department of Transportation
Federal Railroad Administration
Office of Research and Development
1120 Vermont Avenue NW-Mail Stop 20
Washington, DC 20590

10. SPONSORING/MONITORING AGENCY REPORT NUMBER
DOT/FRA/ORD-01/12

11. SUPPLEMENTARY NOTES
U.S. Department of Transportation*
Research and Special Programs Administration
John A. Volpe National Transportation Systems Center
55 Broadway
Cambridge, MA 02142-0193

**Specific computer-simulated figures in this report are available in color on the FRA web site at www.fra.dot.gov

12a. DISTRIBUTION/AVAILABILITY STATEMENT
This document is available to the public through the National Technical Information Service, Springfield, Virginia 22161. This document is also available on the FRA Web site at www.fra.dot.gov

12b. DISTRIBUTION CODE

13. ABSTRACT (Maximum 200 words)

This study assesses the potential safety risks associated with aerodynamic loads produced by the Acela high-speed train when passing freight and bi-level commuter passenger cars. Acela operates at speeds up to 150 mph, on tangent track adjacent to nearby passenger and freight trains. This study was undertaken to determine the effect of the aerodynamic loads generated by Acela on slower moving trains. Past experience has shown that these loads can be substantial and could lead to derailments, dislodgement of freight containers or cause damage to windows of passenger rail cars. Three scenarios have been considered here:

1. The derailment or wheel lift of a container freight car or consist.
2. The breaking loose or dislodgement of shipping containers from a freight consist.
3. The breaking or blowout of windows in a passenger rail car.

This study takes a worst-case approach, where possible, in establishing the aerodynamic loads and the subsequent train response. Therefore, this study determines if such accidents are possible, but does not address whether they are probable.

14. SUBJECT TERMS
Derailment, container dislodgement, aerodynamic load, double-stack container, pressure contours, bi-level passenger rail car, high-speed train

15. NUMBER OF PAGES
72

16. PRICE CODE

17. SECURITY CLASSIFICATION OF REPORT	18. SECURITY CLASSIFICATION OF THIS PAGE	19. SECURITY CLASSIFICATION OF ABSTRACT	20. LIMITATION OF ABSTRACT
Unclassified	Unclassified	Unclassified	

PREFACE

This study assesses the potential safety risks associated with aerodynamic loads produced by the high-speed Acela Express train when it passes freight and bi-level commuter passenger trains. Acela Express operates at speeds up to 150 mph (220 ft/s) on tangent track adjacent to nearby passenger and freight trains. This study was undertaken to assess the effect of the aerodynamic loads generated by Acela Express on these slower trains. Past experience shows that these loads can be substantial and could lead to derailments, dislodgement of freight containers or cause damage to windows of passenger rail cars. Three scenarios have been considered here: 1) the derailment of a container freight car or consist, 2) the breaking loose or dislodgement of shipping containers from a freight consist, and 3) the breaking or blowout of windows in a passenger rail car. This study takes a worst-case approach where possible in establishing the aerodynamic loads and the subsequent train response. This study attempts to understand whether such accidents are possible and not whether they are probable.

This work is sponsored and directed by the Federal Railroad Administration (FRA) through the Volpe National Transportation Systems Center, and James H. Lamond, Technical Monitor. Robert M. Dorer and Harvey Lee of the Volpe Center and Thomas Tsai (FRA) provided additional technical guidance.

METRIC/ENGLISH CONVERSION FACTORS

ENGLISH TO METRIC	METRIC TO ENGLISH
LENGTH (APPROXIMATE)	**LENGTH** (APPROXIMATE)
1 inch (in) = 2.5 centimeters (cm)	1 millimeter (mm) = 0.04 inch (in)
1 foot (ft) = 30 centimeters (cm)	1 centimeter (cm) = 0.4 inch (in)
1 yard (yd) = 0.9 meter (m)	1 meter (m) = 3.3 feet (ft)
1 mile (mi) = 1.6 kilometers (km)	1 meter (m) = 1.1 yards (yd)
	1 kilometer (km) = 0.6 mile (mi)
AREA (APPROXIMATE)	**AREA** (APPROXIMATE)
1 square inch (sq in, in^2) = 6.5 square centimeters (cm^2)	1 square centimeter (cm^2) = 0.16 square inch (sq in, in^2)
1 square foot (sq ft, ft^2) = 0.09 square meter (m^2)	1 square meter (m^2) = 1.2 square yards (sq yd, yd^2)
1 square yard (sq yd, yd^2) = 0.8 square meter (m^2)	1 square kilometer (km^2) = 0.4 square mile (sq mi, mi^2)
1 square mile (sq mi, mi^2) = 2.6 square kilometers (km^2)	10,000 square meters (m^2) = 1 hectare (ha) = 2.5 acres
1 acre = 0.4 hectare (he) = 4,000 square meters (m^2)	
MASS - WEIGHT (APPROXIMATE)	**MASS - WEIGHT** (APPROXIMATE)
1 ounce (oz) = 28 grams (gm)	1 gram (gm) = 0.036 ounce (oz)
1 pound (lb) = 0.45 kilogram (kg)	1 kilogram (kg) = 2.2 pounds (lb)
1 short ton = 2,000 pounds (lb) = 0.9 tonne (t)	1 tonne (t) = 1,000 kilograms (kg)
	= 1.1 short tons
VOLUME (APPROXIMATE)	**VOLUME** (APPROXIMATE)
1 teaspoon (tsp) = 5 milliliters (ml)	1 milliliter (ml) = 0.03 fluid ounce (fl oz)
1 tablespoon (tbsp) = 15 milliliters (ml)	1 liter (l) = 2.1 pints (pt)
1 fluid ounce (fl oz) = 30 milliliters (ml)	1 liter (l) = 1.06 quarts (qt)
1 cup (c) = 0.24 liter (l)	1 liter (l) = 0.26 gallon (gal)
1 pint (pt) = 0.47 liter (l)	
1 quart (qt) = 0.96 liter (l)	
1 gallon (gal) = 3.8 liters (l)	
1 cubic foot (cu ft, ft^3) = 0.03 cubic meter (m^3)	1 cubic meter (m^3) = 36 cubic feet (cu ft, ft^3)
1 cubic yard (cu yd, yd^3) = 0.76 cubic meter (m^3)	1 cubic meter (m^3) = 1.3 cubic yards (cu yd, yd^3)
TEMPERATURE (EXACT)	**TEMPERATURE** (EXACT)
[(x-32)(5/9)] °F = y °C	[(9/5) y + 32] °C = x °F

QUICK INCH - CENTIMETER LENGTH CONVERSION

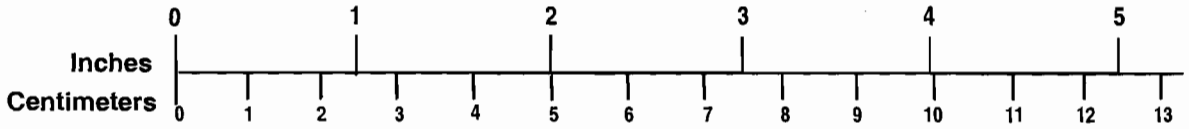

QUICK FAHRENHEIT - CELSIUS TEMPERATURE CONVERSION

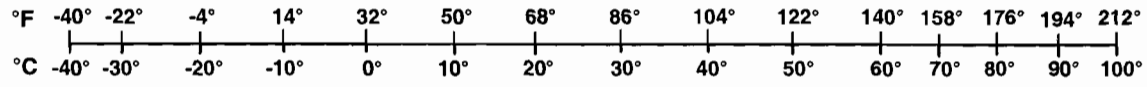

For more exact and or other conversion factors, see NIST Miscellaneous Publication 286, Units of Weights and Measures. Price $2.50 SD Catalog No. C13 10286

Updated 6/17/98

TABLE OF CONTENTS

LIST OF FIGURES

LIST OF FIGURES (cont.)

LIST OF TABLES

EXECUTIVE SUMMARY

The objective of this study was to examine the aerodynamic interaction of passing trains, and assess the potential dangers of train derailment or dislodgement of double-stack container cars, as well as the damage to windows of bi-level commuter cars. This study focuses on scenarios in which an Acela Express trainset is moving at a high rate of speed and passes a slower freight or passenger train. Under these conditions, the greatest changes in aerodynamic load are generated on the cars in the slower train. The problem that was caused by the high-speed Acela Express train as it passed the slower freight consist was examined using Acusolve™ and NUCARS[1] computer codes. Acusolve™ is a finite element code for incompressible flow problems, and is used to calculate aerodynamic loading. NUCARS is a train motion simulation program that is used to determine the resultant motion and risk of derailment of the slower train consist. The problems of container dislodgement and window breakage are analysed using computed aerodynamic loads.

A total of 15 aerodynamic scenarios were used to investigate the loads on the container train using Acusolve™. These calculations show that the maximum aerodynamic loads on the container train occur when it passes the leading and trailing end of Acela Express. The container cars were subjected to strong lateral push-pull forces causing both rolling and yawing moments, as well as lateral displacements of the freight cars.

The potential for container consist derailment was investigated for each aerodynamic load condition. The dynamic response of both empty and loaded freight container consists were analyzed for a string of five articulated cars using shared trucks. NUCARS' results show that for articulated cars carrying empty containers, the potential for derailment does exist. The risk of derailment was lower when the freight consist carried full or partially loaded containers. The worst-case occurred when high lateral ambient wind speed was combined with the aerodynamic forces created at the ends of an Acela Express, which produced freight car wheel unloading, and had the potential for derailment. Some improvement was noted when the container train was carrying fully loaded containers, but even in these cases a risk still remained for some operating scenarios.

The problem of container dislodgement was examined by calculating the aerodynamic loads on individual containers. Based on specified tie-down strengths for shipping containers, it does not appear that a properly restrained container would break loose under the conditions investigated in this study. However, it might be prudent to increase the required tie-down strength for lateral loads, for an added safety margin. Two separate aerodynamic calculations simulating a typical bi-level commuter car being passed by an Acela Express were performed to address the question of window damage and blowout. These analyses suggest that window blowout or breakage is unlikely; however, a more detailed structural analysis including quantification of window glazing strength variation is needed in order to answer this question more conclusively.

To ensure proper safety, consideration must first be given to the results of these case studies. Careful consideration must also be given to the likelihood that rare combinations of operating

[1] NUCARS is a trademark of the Transportation Technology Center, Inc., Pueblo, Colorado.

circumstances may have adverse effects on the freight consist and the Acela Express train. An analysis of operating rules, traffic patterns and weather cycles pertinent to conditions in areas of operation could be performed to quantify the relative statistical probability of loading scenarios examined in this study.

1. INTRODUCTION

The purpose of this study was to examine the potential safety hazards to existing rail traffic operating in the Northeast corridor from aerodynamic loads generated by the Acela Express high-speed passenger train. Several scenarios have been examined here with the objective of assuring the safety of both Acela Express and other trains operating on adjacent tracks. Three scenarios were considered: 1) the derailment of a freight container consist when passed by Acela Express, 2) the breaking loose or dislodgement of shipping containers from the freight container car and, 3) the breaking or blow-out of windows in a passenger train when passed by Acela Express.

Large aerodynamic loads can be generated when two trains pass one another. The magnitude and duration of the load depends on the velocity and geometry of the two trains, the track spacing, and also the ambient wind speed and direction. The first sections in this report focus on the first and perhaps most difficult problem of derailment. The aerodynamic calculations are described first, and are followed by a description of the resulting train dynamics and derailment analysis. Concluding sections of the report discuss the analysis of container dislodgement and window damage.

The objective of this study was to determine if aerodynamic loads generated by Acela Express act on trains using adjacent track, and the potential safety risks. A worst-case approach was taken, where possible, in establishing the aerodynamic loads and subsequent train response. This study was performed using the Acusolve™ and NUCARS computer codes. Aculsove™ is a computational fluid dynamics (CFD) code for solving incompressible flow problems. NUCARS is a train dynamics simulation program for determining the resultant motion and risk of derailment of passing trains.

In order to facilitate the computational process, the aerodynamics calculations were separated from the dynamic response calculations. The implied underlying assumption is that the small response motions of the container train or passenger train will not influence the aerodynamic loads. A matrix of aerodynamic calculations were used to characterize the loads on the passing trains (either a container consist or a passenger car), in terms of peak force and moment resultants as well as load duration or total impulse.

Two types of trains that could be met by Acela Express in the Northeast corridor were chosen for detailed analysis as part of this study. The first was a double-stack container car in a 5-pack articulated consist. This consist is characterized by a large surface area with a propensity for dynamic interaction between cars with shared trucks. For passenger applications, a contemporary bi-level commuter rail car was chosen because it also has a large surface area with large windows and is representative of car types encountered by Acela Express. Much of this report focuses on the analysis of freight car response with regard to the potential for derailment. The potential for passenger rail car window blowout and individual freight-container dislodgement were examined by comparing the predicted aerodynamic forces with static safe load limits for these components.

The container cars studied utilized shared trucks, which are combined in an articulated string of a 5-car pack as shown in Figure 1. Each container car has an effective length (truck-to-truck center distance) of 58 ft 10 in. (18.7 m). In Figure 1, the near car has a single container mounted over a second shorter container. The lower container sits in the well of the container car. As a worst-

case, a 53-ft (16-m) long container mounted over a single 40-ft (12.2-m) container was selected. This type of container arrangement results in a staggered end on the container stack similar to that shown in Figure 1, where the length of the top container is the largest permissible. The stack has a total height above track level of about 16 ft (4.9-m) and presents a large lateral surface area to Acela Express, so that small changes in lateral pressure give rise to large lateral forces.

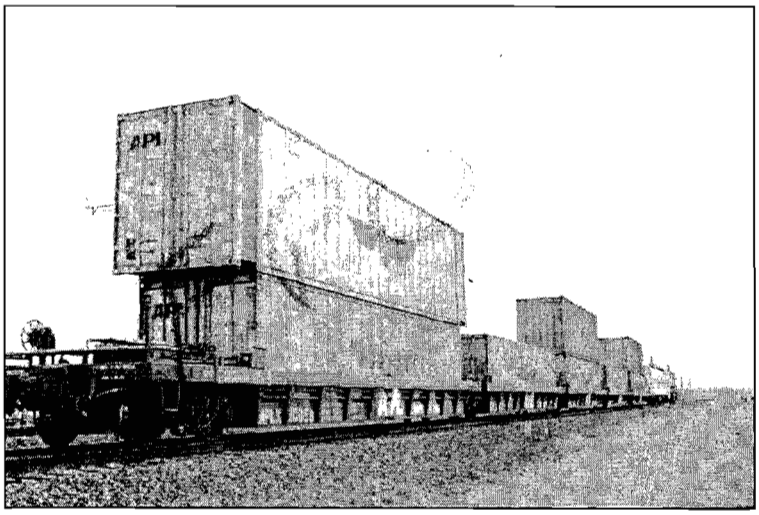

Figure 1. Generic Double-stack Container Car with Containers

This study has confined its analyses to empty and loaded container cars with a general configuration as seen in Figure 1. For many of the aerodynamic calculations it was assumed that the upper and lower containers were the same length, which created a single vertical edge at the container ends. This arrangement gave rise to slightly higher predicted loads on the container car than arrangements with a staggered end. The NUCARS' results were obtained from a model of the complete 5-car freight consist including details associated with shared-truck articulated joints.

2. CONSIST RESPONSE STUDY

2.1 AERODYNAMIC LOADING

The response of the container consist depends on the magnitude, direction, and duration of the aerodynamic load. The problem attributed to passing trains is made complex by the need to model the large relative movement of the two trains and by the wide range of parameters that must be explored. The aerodynamic loads are functions of the speed and direction of the two trains and the ambient wind speed and direction. This study focuses on how the variation in these parameters affects the loads on the container train and its response. This requires a large analysis matrix in order to define the relationship between operating conditions and load as well as the effect of the dynamic loads on container train response. In order to keep the computational expense of these calculations reasonable, the aerodynamic portion of the problem was modeled as an Euler equation (potential flow), rather than a viscous flow problem. This was accomplished by using relatively course grids, and no turbulence model. Thus, the drag on an Acela Express trainset, and the container train is not captured accurately in these solutions and the emphasis is placed on the dynamic or changing loads. This is acceptable because the calculations show that the drag obtained by integrating the pressure over the surface of the container car constitutes nearly all of the important dynamic loads that might lead to derailment. It will be shown that the lateral load component will most likely affect derailment, and the axial load component, which arises principally from the steady aerodynamic drag, is relatively unimportant.

2.2 AERODYNAMICS APPROACH

The aerodynamic loads on the container train are calculated using the Acusolve finite element based computational fluid dynamics (CFD) solver. Acusolve™ uses unstructured grids enabling easier mesh generation. Two meshes representing a course and fine discretization were generated to model the contours of Acela Express and a container train on an adjacent track. The course mesh contains 92,682 hexahedral elements and 99,834 nodes, and the fine mesh contains 305,868 hexahedral elements and 321,609 nodes. Figure 2 shows the overall mesh shape. The mesh, representing the fluid around Acela Express and the container train, is a parallelepiped with dimensions of 230 ft long by 115 ft wide by 66 ft high (70 m x 35 m x 20 m). The mesh originates at the front of Acela Express at the track level, while Acela is facing in the positive X-direction. The container train is to the left of Acela Express in the positive Y-direction, and the positive Z-direction is upwards as shown in Figure 2. The track spacing is 12 ft (3.658 m) from centerline to centerline.

The course and fine meshes are fixed to represent the surfaces of the Acela Express and the container cars. However, the effect of containers themselves is modeled using a moving boundary condition that will be described later in this section. Figure 3 shows a closer view of the surface mesh on Acela Express and the container cars for both meshes. Note that the mesh is refined near the nose of Acela Express for both the fine and coarse meshes. Also, the track ballast contours are modeled in both meshes, and the fine mesh includes the track contours under the two trains. As a simplification, the open space under the two trains is modeled as a simple passage and no details of the trucks or undercarriage are shown. The spaces between the container cars are not modeled.

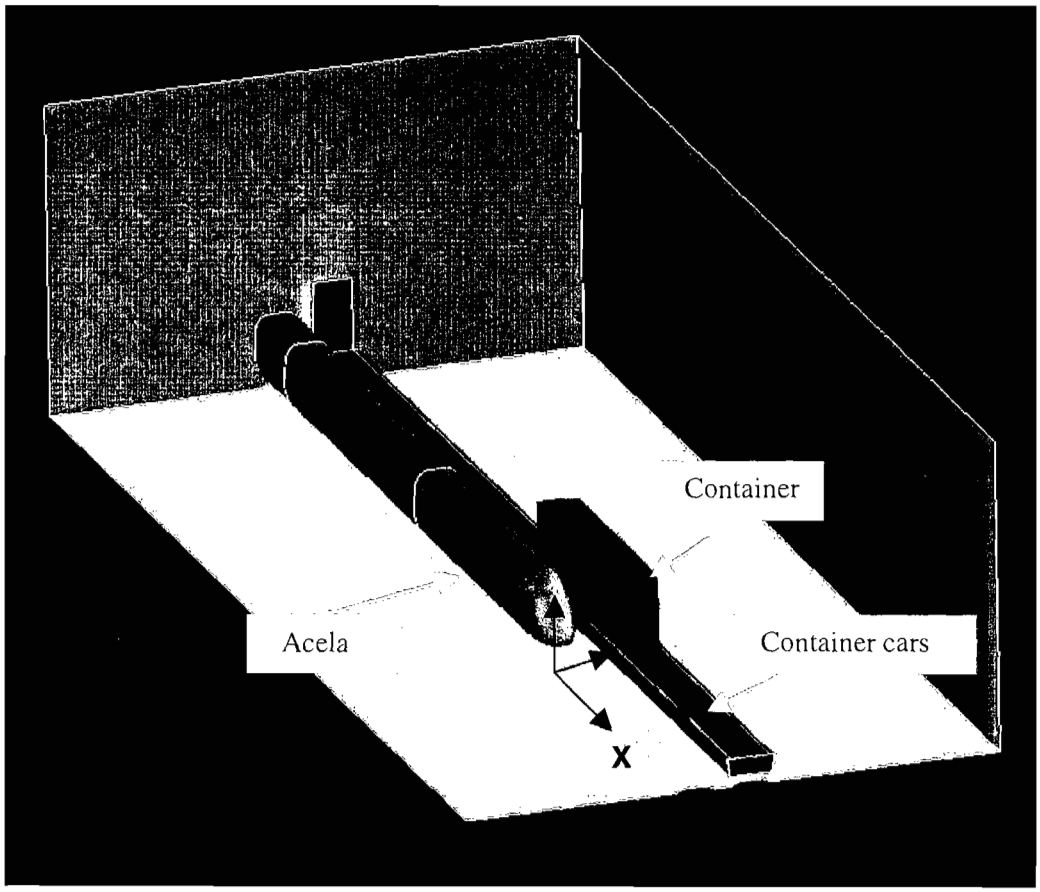

Figure 2. Fluid Volume of CFD Mesh

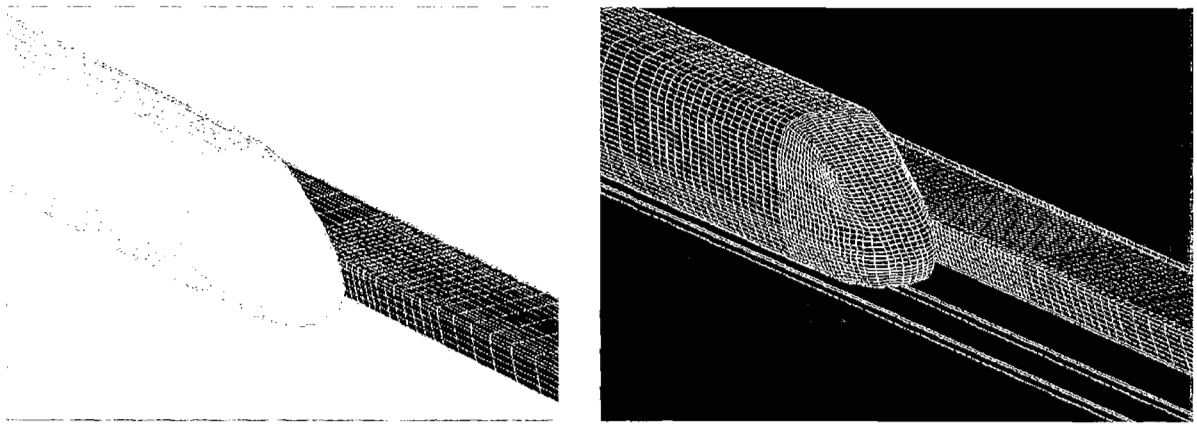

Figure 3. Coarse (left) and Fine (right) Mesh Surfaces

In the approach used here, the fluid mesh is fixed so that all velocity boundary conditions for the CFD solution are specified relative to the Acela Express velocity. The motion of the

container(s) relative to Acela Express is modeled as a moving boundary condition, i.e., as a boundary condition on the nodes in the area above the container car. In this approach, the effect of the container(s) is moved through the mesh while the mesh remains fixed. As nodes enter the container volume, the boundary condition is applied so that the fluid velocity within the container is constrained to be the container velocity. Thus, the momentum of the fluid within the moving boundary is constant and the pressure distribution on the boundary surface is the same as would occur if the boundary condition (i.e., the container velocity) were applied to the nodes defining the container surface. The boundary condition is illustrated in Figure 4. Note that the boundary condition is sometimes applied over a few time steps in order to reduce pressure fluctuations in the mesh. These fluctuations arise when several nodes enter the moving boundary at the same time, as seen for the configuration shown in Figure 4.

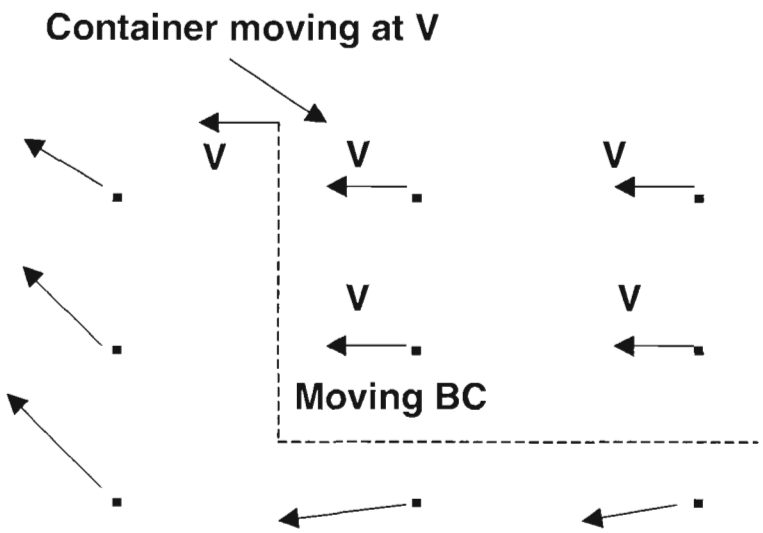

Figure 4. Moving Boundary Condition

Two different configurations of the moving boundary condition are used to represent containers in the consist. These are shown in Figure 5. The configuration on the left (a) is for a simple rectangular container, while the configuration on the right (b) uses a staggered end for the container. By comparing simulations using the two configurations, it was found that the simple configuration gave slightly higher loads on the container car. This configuration was used for most of the derailment study. The staggered configuration of (b) gives slightly higher loads on the top container and is used in the dislodgement study.

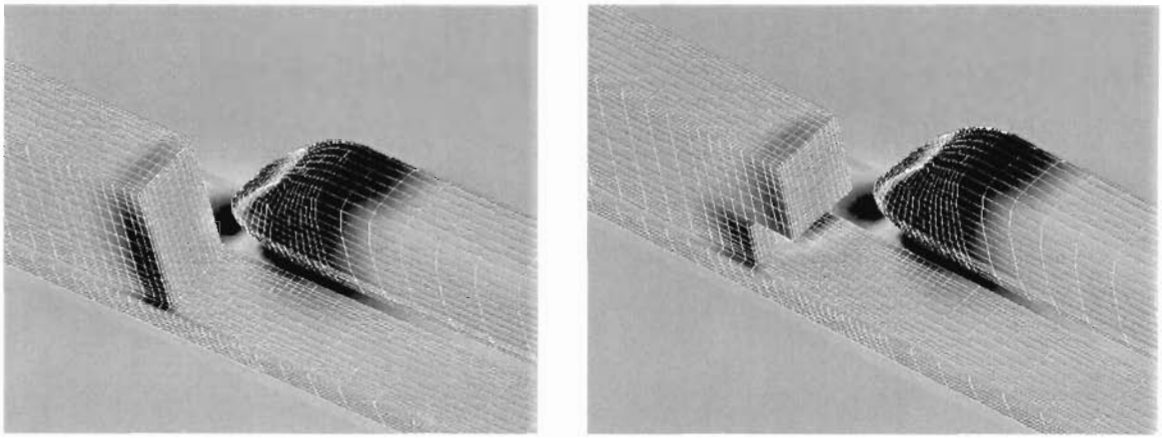

(a) Simple end (b) Staggered end

Figure 5. Container Configurations Shown with Pressure Contours

2.2.1 EXAMPLE CALCULATION

The scenario of Acela Express meeting a container train moving in the opposite direction is used here to illustrate the basic features of the interaction problem and the data reduction procedure. In this first case, Acela Express is moving at a velocity of 150 mph (219 ft/s) towards a container train moving in the opposite direction at 50 mph (73 ft/s) in still air. With a closing speed of 200 mph (293 ft/s), the 61.3 ft long container car passes a fixed point on Acela Express in 0.21 seconds.

The solution for this example (later referred to as Case 1) was obtained using the coarse mesh and 150 time steps of 0.005 seconds each. After completion, the solution was post-processed to examine the flow and to obtain pressure contours on the surface of Acela Express and the container train. In addition, integrating the surface pressure over the car and container surfaces derived the load history on the container car. This analysis showed an interaction pattern that is repeated for all of the analyses completed. However, the magnitude and duration of the load and some of the load features change with the expected problem parameters.

The sequence of events occurring at the front-end of Acela Express as it meets the container is illustrated in Figure 6. This figure consists of a sequence of six pictures taken at evenly spaced intervals during the passing process. In this example, a single loaded container car in a string of unloaded cars passes the front-end of the Acela Express. As seen in the first frame, the highest pressures occur on the front of Acela Express, which is moving at 150 mph (220 ft/s). As Acela moves ahead, a high-pressure region is driven in front of the cab (red contours) and low-pressure regions form on the flanks of the cab. The stagnation pressure for Acela Express is 0.39 psi, so that the pressure over much of the nose of Acela Express is at 0.22 psi or above.

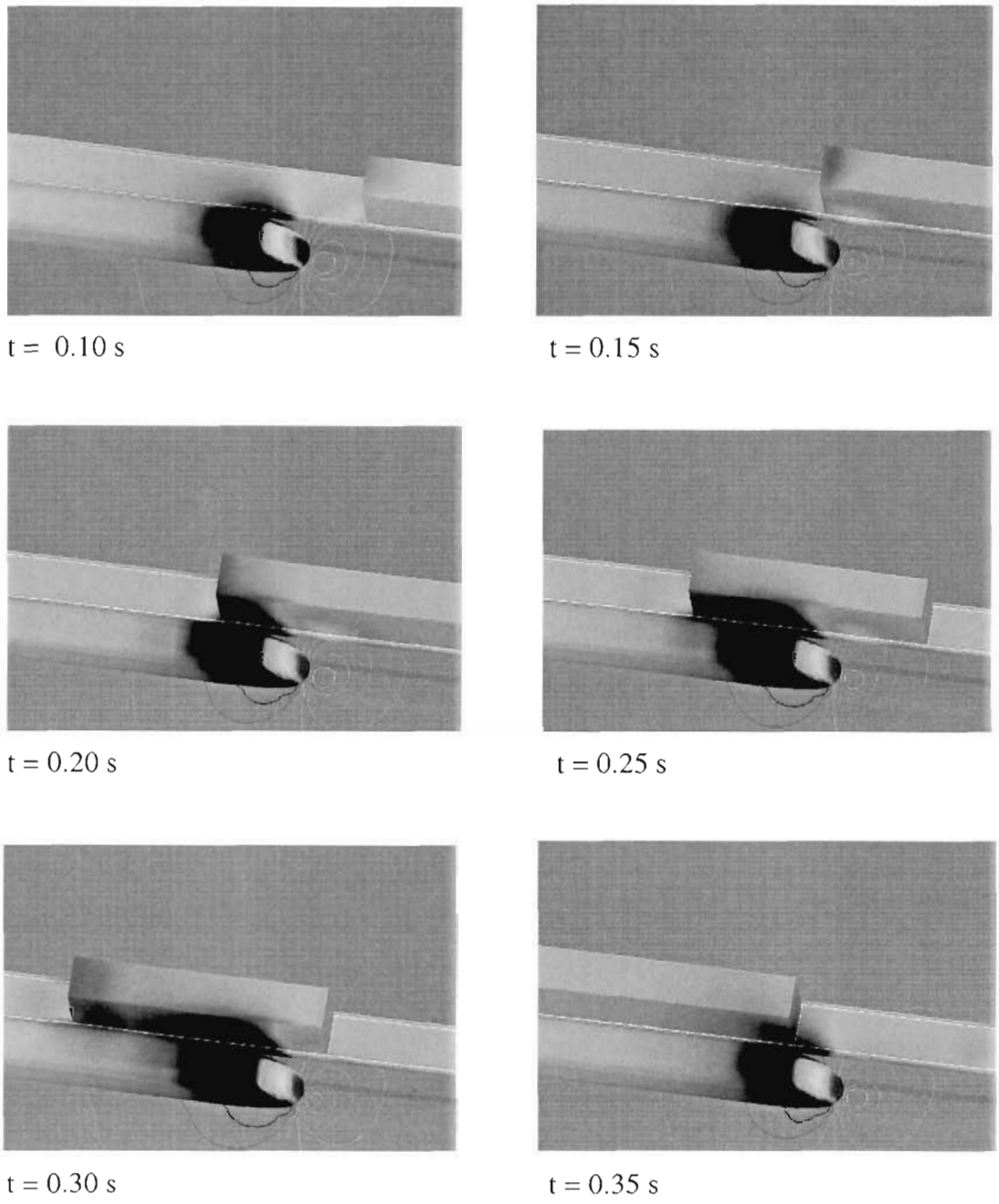

Figure 6. Pressure Contours on Acela Express and Container Consist for Case 1

Contour range from –0.073 psi to +0.22 psi

The second frame of the sequence shows the interaction between the trains after Acela Express has passed the front-end of the container car. The bubble of high-pressure in front of Acela Express is pushing the front of the container car away from Acela Express in the plus-Y direction. As the passing sequence progresses, the high-pressure region moves back along the side of the container car and the front of the car is pulled towards Acela Express by the low-pressure region alongside the Acela Express cab. Later in the sequence, the back-end of the container car is pulled towards Acela Express by the low-pressure region. Thus, the container car and Acela Express both experience a rapid lateral push-and-pull force along with yawing moments.

The force and moment resultants on the container were evaluated by integrating the pressure on the surface of the container moving boundary. The reference frame used to calculate the forces and moments is illustrated in Figure 7. Here, the xyz coordinate system is fixed to the center of the container car at the track level. The x-y plane is at the track level with z representing the vertical axis. The wind velocity components (used later) are given in the same (x-y-z) coordinate frame. The force and moments on the container car are taken with reference to a point at the center of the car at rail height, as shown in Figure 7. The forces and moments are captured as functions of time from the flow calculation by integrating the pressure histories on the car surface at each time step. These force and moment histories are presented in Figure 8.

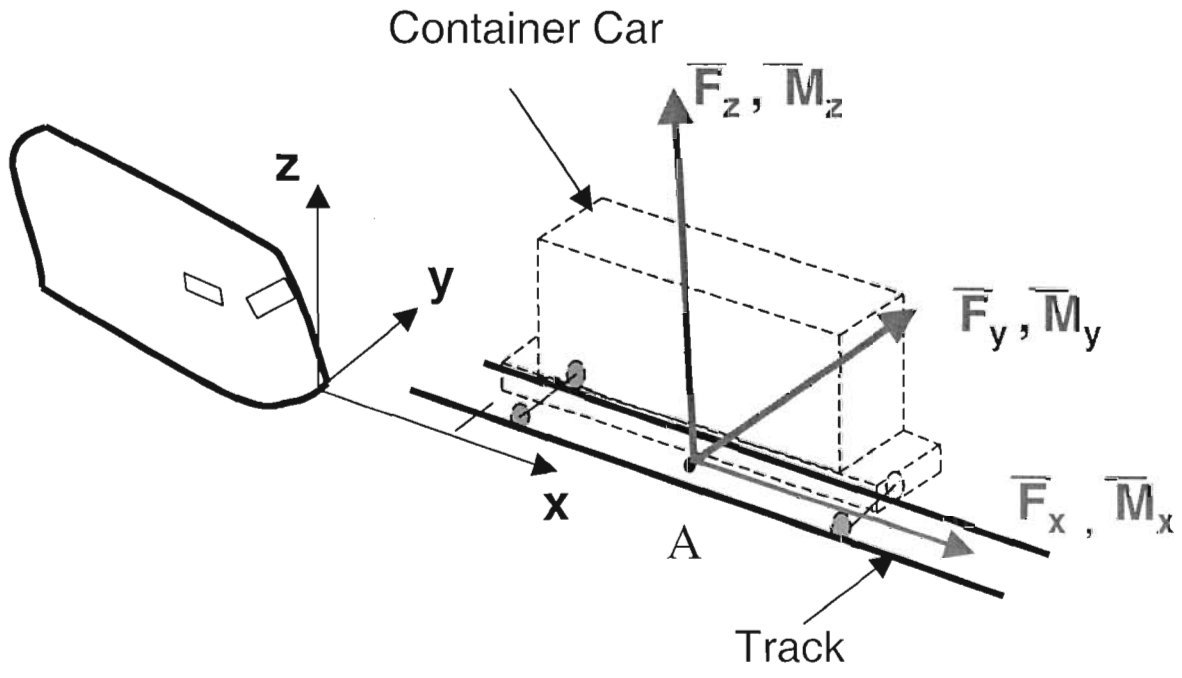

Figure 7. Axis Definition for Forces and Moment Resultants

The lateral force F_y shown in Figure 8 shows the push-pull effect as a result of the freight-consist passing the nose of Acela Express. In Figure 8, t1 indicates the time when the front of the container car reaches the front of Acela Express, and t2 is the time when the back of the container car reaches the front of Acela Express. The overall effect on the container car is to exert a force away from Acela Express at the front of the container car as seen by the lateral force (F_Y). This produces a positive force in the Y direction that reaches a peak at 0.16 seconds. During this phase there is also a negative rolling (M_X) moment that is similar in shape. There is also a small negative (Z) or yaw moment which reaches a minimum at 0.16 seconds. As the container moves further past Acela Express it approaches the low-pressure region around the cab, so the net force in the y direction drops. The Z or yaw moment increases to a maximum under the combined effect of the high-pressure region ahead of Acela Express and the pressure region around the cab. The time now is 0.24 seconds. The lateral force decreases to a minimum at the same time the back of the container car enters the low-pressure region. The roll and yaw moments reflect this change as well. During this entire process, the longitudinal and vertical loads on the container car remain small and can probably be neglected when considering the motion of the entire container car.

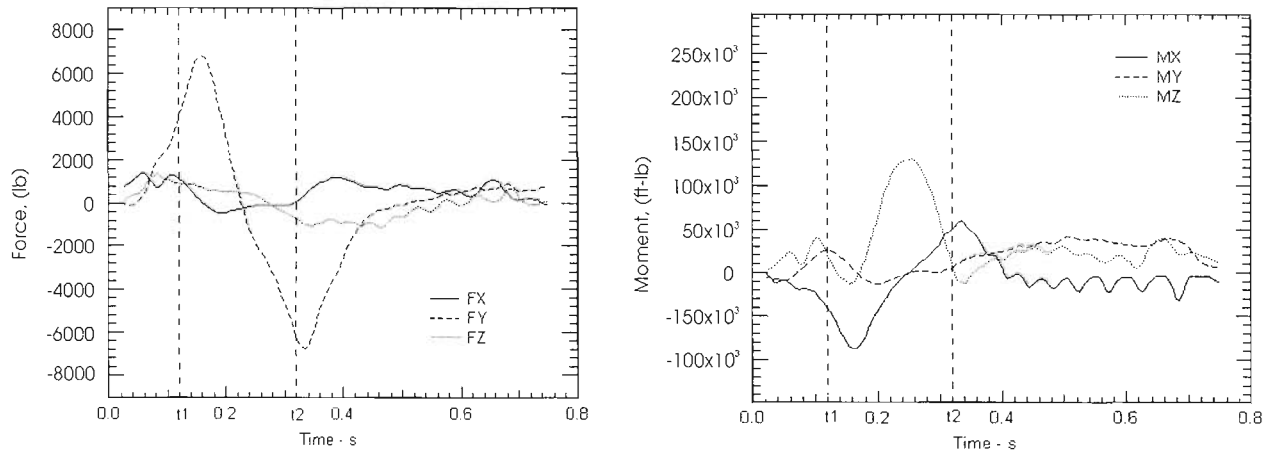

Figure 8. Forces and Moments on Container Car for Case 1

It should be noted that the effects of the moving boundary and the integration of the pressure over the boundary from time step to time step may produce some unevenness or jitter in the force and moment diagrams. Using the binomial smoothing method described in Reference 1, the force and moment histories where jitter might occur were smoothed in order to make interpretation of the data easier. The forces and moments for the first 10 time steps were also suppressed or damped to eliminate jitter, which occurred during the start of the solution. These data reduction procedures and their effects are discussed in Appendix A.

After the initial interaction of the container car on the front-end of Acela Express, the container car moves to the long uninterrupted side of Acela and the forces and moments on the container car subside, but do not go to zero. Later in the sequence, the container car encounters the tail-end of Acela Express and a new dynamic interaction takes place. This

second interaction was modeled in a separate calculation, obtained by reversing the flow and container motion directions within the same mesh.

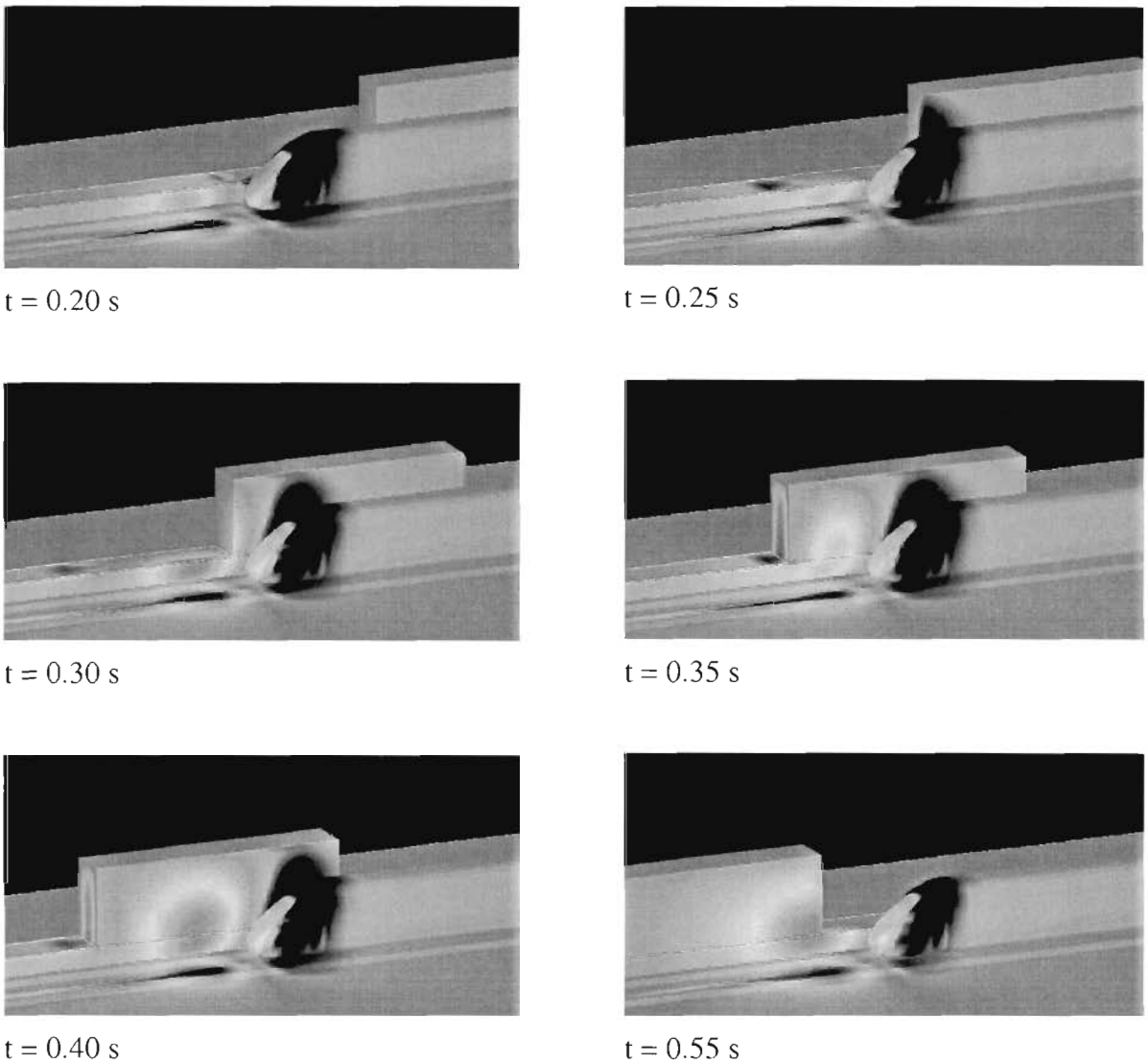

Figure 9. Pressure Contours on Acela Express and Container During Interaction at the Back-end of Acela Express

Contour range from –0.073 psi to +0.073 psi

Figure 9 shows the pressure contours on the Acela Express and the container train during interaction at the back-end of Acela Express. Note that the mean pressure levels in this calculation are not matched to those used at the front-end of Acela Express, so that the maximum pressures indicated should not be compared directly to those in Figure 6 by comparing contour bands. Furthermore, because the turbulence model is not being used, the pressure in the wake of Acela Express is somewhat suspect, as turbulence effects should reduce the pressure recovery in the wake. Nevertheless, it is believed that this flow

calculation gives a good approximation of maximum dynamic loads that might be expected at the back-end of Acela Express. Figure 10 shows the integrated pressure resultants on the container car for the interaction at the back-end of the Acela Express.[1]

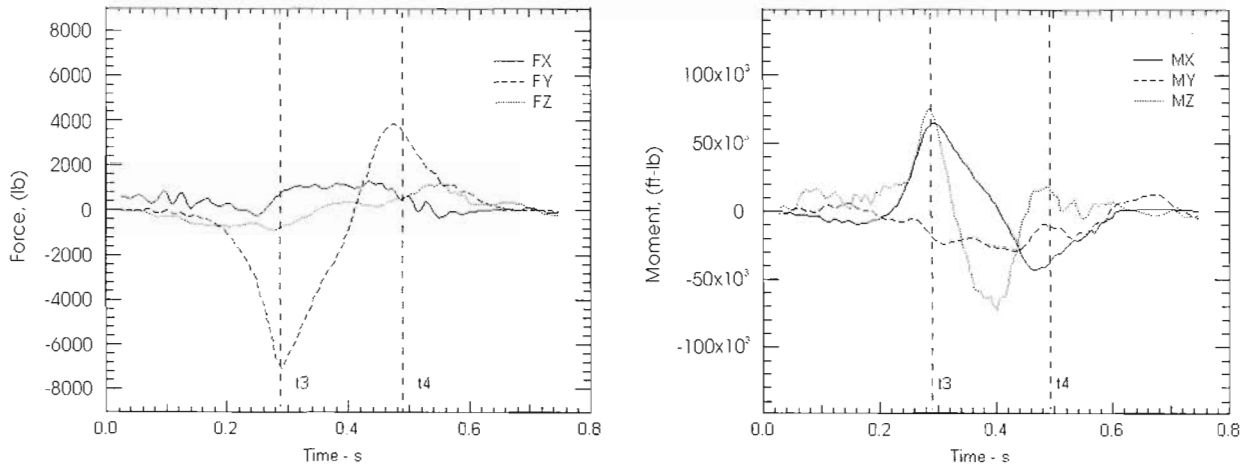

Figure 10. Forces and Moments on Container Car During Interaction at Back End of Acela Express

2.2.2 AERODYNAMIC ANALYSIS MATRIX FOR CONTAINER CARS

It is believed that the primary variables affecting the aerodynamic loads are: 1) the velocities of Acela Express and the container train, and 2) the ambient wind direction and speed. Secondary variables that may affect aerodynamic loading are small changes in container geometry and the arrangement of the containers. Several cars stacked on containers in rows, or a single container surrounded by empty cars could also affect aerodynamic loading. The CFD analysis matrix, which is shown in Table 1, was chosen to provide a wide variation of the primary variables with some variations of the secondary variables. Note that Acela Express is always moving ahead in the positive X-direction. Positive velocities for the container train indicate that it is moving in the same direction as Acela Express, while negative X components of wind velocity are identified as Acela Express headwinds. A negative value of the Y-component of wind velocity is directed from the container train toward Acela Express.

The matrix of aerodynamic calculations was planned to cover a range of operation and ambient conditions, and also to explore potential worst-cases from the point of view of aerodynamic interactions as well as from the container consist response. A total of 15 calculations were completed that modeled the overall forces on a container consist. These are listed in Table 1 as Cases 1-15. The second column in the table provides the location of the Acela Express and container car interaction, indicating whether it occurred at the front or back-end. The third and fourth columns contain the shape and number configuration that refers to container and consist arrangement, respectively. For example, the simple (S) type shape represents the container arrangement of that shown in Figure 5a, and the complex shape of that shown in Figure 5b. Each of the 15 cases listed in Table 1 were analyzed using

[1] Illustrations at the back of Acela Express use the same reference frame as was used at the front of Acela.

the methods described in Section 2.2.1. Appendix C contains the force and moment diagrams for each of the 15 cases. The last two columns in Table 1 give values for the maximum change in lateral force (maximum force minus minimum force), and the maximum absolute value for lateral impulse. This last value was obtained by numerically integrating the lateral force (F_Y) time history.

The conditions outlined in Table 1 were planned to cover a range of train and wind speed variables. Cases 1 to 9 focus on the extremes in passing velocity with Acela Express and the container consist at maximum speed. These cases also include the effects of ambient wind including a 50 mph headwind and tailwind for Acela Express, and a 50 mph crosswind. In general, it was found that the dynamic lateral load between vehicles was maximized when Acela Express faced a headwind and minimized when Acela Express faced a tailwind. In the case of a headwind, where the closing speed between vehicles was 200 mph (Case 5), the peak-to-peak change in lateral load was 96,000 N or about 21,500 lbf (Figure 11).

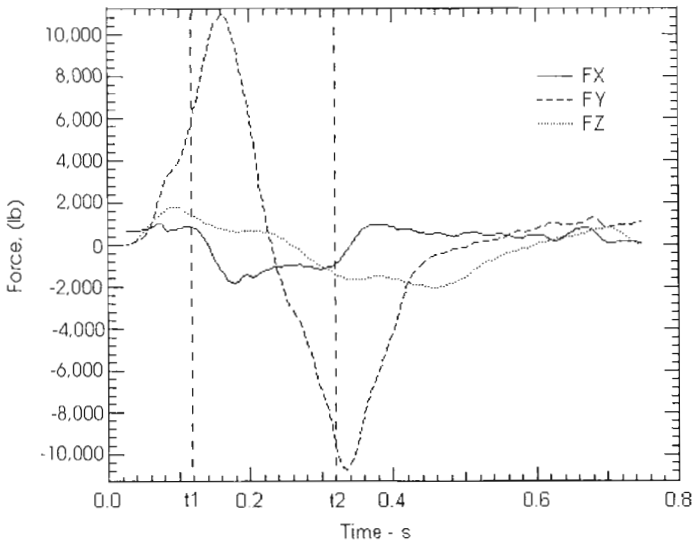

Figure 11. Force Histories on Container from Case 5; the Effect of Headwind

Table 1. CFD Analysis Matrix for Container Consists

Case	Location [1]	Container Configuration		Train Velocity		Wind		Aerodynamic Load	
		Type[2]	Number[3]	Acela Express (mph)	Container (mph)	V_x (mph)	V_y (mph)	Maximum change in lateral force (N)	Max. absolute lateral impulse (N-s)
1	F	S	1	150	-50	0	0	61,000	2,700
2	F	S	3	150	-50	0	0	52,000	2,120
3	R	S	1	150	-50	0	0	48,200	3,470
4	F	C	1	150	-50	0	0	44,000	2,110
5	F	S	3	150	-50	-50	0	96,000	4,500
6	F	S	1	150	-50	50	0	33,700	1.260
7	F	S	1	150	50	50	0	23,900	2,350
8	F	S	1	150	50	-50	0	73,000	8,410
9	F	S	1	150	-50	0	-50	38,300	-
10	F	S	1	150	30	50	0	23,900	2,000
11	F	S	1	150	15	50	0	26,700	1,820
12	F	S	1	150	30	-50	0	77,900	8,190
13	F	S	1	150	15	-50	0	81,500	7,060
14	R	S	1	150	50	-50	-50	40,000[4]	-
15	F	S	1	120	50	-50	0	54,600	11,020

1. Refers to location of interaction – either at the front or back of Acela Express.
2. Shape of container end, either simple (S) with top and bottom containers of same length or complex (C) with bottom containers of different lengths.
3. Number of loaded container cars in a row.
4. Reduced time interval.

Conversely, a transverse wind can result in a large static transverse aerodynamic load component. In Case 9 for example, the container was traveling at 50 mph (73 ft/s) with a 50 mph crosswind. Thus, it faced a diagonal wind at a speed of 70.7 mph (104 ft/s). The predicted resultant mean lateral force on the container car during the interaction was on the order of 13,500 lbf (60,000 N) as seen in Figure 12. The dynamic component of the load caused by passing trains alone is 8,600 lbf (38,500 N) quite a bit less than the change in transverse load in Case 1 (13,700 lbf or 61,000 N) where Acela Express and the container train were in still air.

It was also discovered that the impulse on the container consist depended not only on train speed and wind speed, but also to a great extent on train direction. When the container train and Acela Express were moving in the same direction, they interacted for a longer period of time and the impulse increased even though the peak loads may have decreased slightly. Although the shape of the force resultant histories were similar when the two trains were moving in the same direction, the duration of the loads increased in proportion to the time of interaction. This effect can be seen in Figure 13,which compares the lateral forces in Cases 5 and 8. In both cases, Acela Express faced a 50 mph headwind. In Case 5, the container train was moving at 50 mph in the opposite direction. In Case 8, Acela Express and the container train were traveling in the same direction. Integrating these curves over the time of contact with the freight car shows that the lateral impulse in Case 8 was greater, but the maximum force was lower.

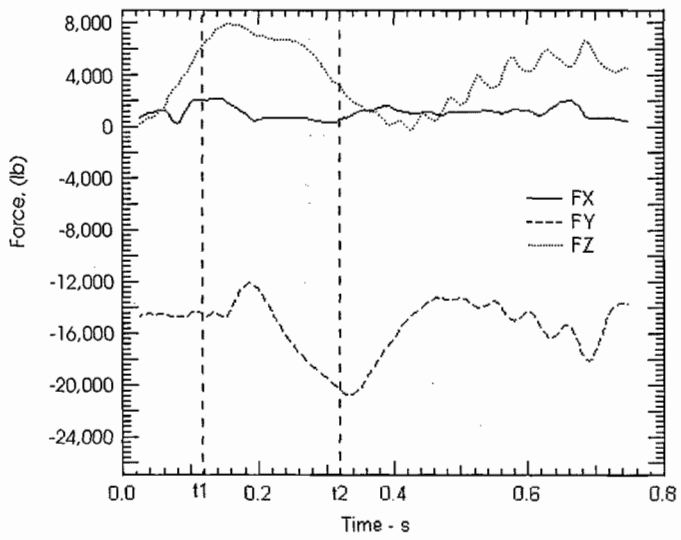

Figure 12. Force Histories on Container from Case 9; the Effect of Crosswind

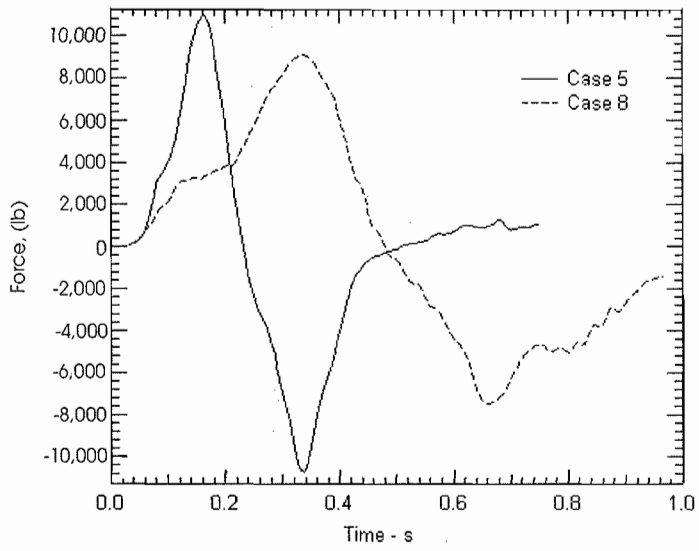

Figure 13. Lateral Force Predicted for Case 5 and Case 8 Showing the Effect of Container Consist Speed and Direction

The calculation of container consist response led to the conclusion that there is a potentially strong interaction between the timing of the load and consist response. NUCARS' calculations, which will be discussed in later sections, show that when the container train and Acela Express move in the same direction, the characteristic load period is closer to the natural period of consist response. This dynamic interaction may be more dangerous. As a result, calculations for Cases 10 to 15 were chosen to examine the effect of load duration on response.

Comparison of the various runs led to the following general conclusions: 1) The highest loads occurred in cases of high train speeds when Acela Express is facing a headwind. 2) The speed of Acela Express is more important than the speed of the container-consist in determining peak load. 3) The duration of load and the impulse are not just functions of train speed, they are also relevant to the direction in which the container-consist travels. 4) If the container-consist is moving in the same direction as Acela Express, then the load duration and lateral impulse is increased. In order to obtain a quantitative measure of this effect, the lateral force history was integrated with respect to time for several cases. The results are shown in Figure 14. Note that in Cases 1, 5, and 6, Acela Express and the container train are moving in opposite directions. In the remaining cases, they are moving in the same direction at various closing speeds. The greatest impulse occurs in Case 8 when Acela Express faces a headwind and the container-consist moves in the same direction at a maximum speed of 50 mph. The effect of headwind on Acela Express can be seen by comparing Case 6 with Case 5. In Case 6, Acela Express has a 50 mph tailwind; in Case 5 it faces a 50 mph headwind.

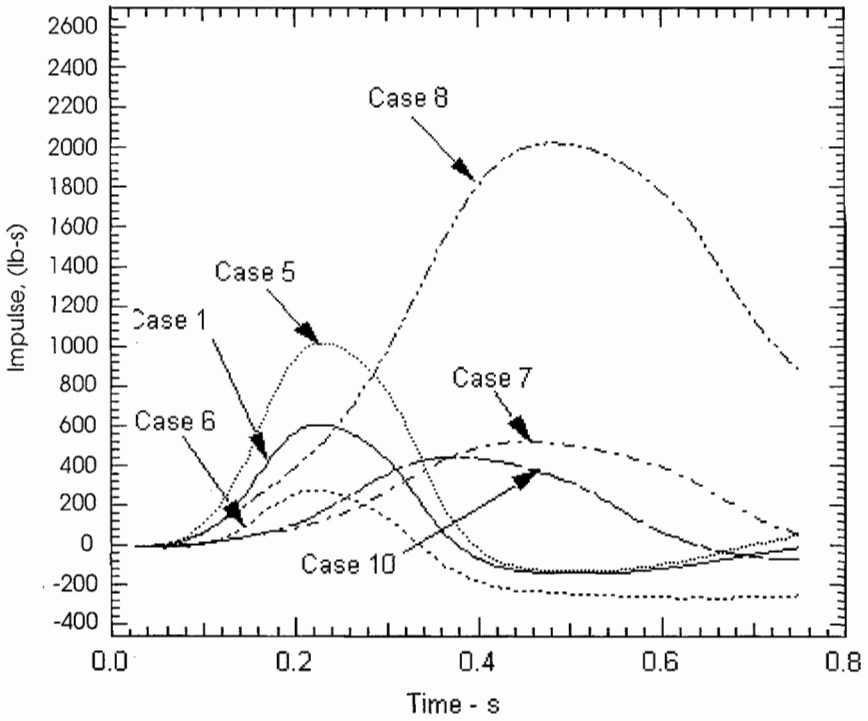

Figure 14. Impulse Histories

2.3 CONTAINER CONSIST DYNAMIC RESPONSE

It is believed that vehicles posing the highest risk for derailment or dynamic instability due to aerodynamic forces are those with large surface areas and lightly damped and coupled dynamical behavior. The typical double-stacked container car in a 5-pack articulated connection, loaded with two levels of containers as seen in Figure 15, has a large surface area and exhibits strong dynamic interaction between cars. In this section, a series of NUCARS simulations were used to assess the risks to double-stacked container cars associated with high-speed passes of the Acela Express train. Quantitative output parameters were used such as wheel lateral to vertical load ratios, vertical wheel loads, and general dynamic behavior of car bodies to assess the risk of derailment.

2.3.1 CONSIST DYNAMICS APPROACH

In each NUCARS simulation, aerodynamic loads acting on the container freight train were taken directly from the CFD calculations, as described in the preceding section. A series of NUCARS modeling studies were performed to assess the dynamic stability of freight trains in the presence of aerodynamic loads caused by high-speed trains passing on nearby parallel tangent track.

The NUCARS computer model is a general-purpose code simulating the time domain response of vehicle rigid-body and flexible-body dynamic modes. The model allows for a wide variation in specified load environments such as the inclusion of wind vectors, inter-body connections, gravity, and other forces or moments. NUCARS is also well adapted to simulate the nonlinear interaction forces produced at wheel and rail contact areas, and is recognized as one of the preeminent models to effectively analyze these interactions. The particular car models used in this study were similar to vehicles previously verified against actual test data collected from

force-instrumented wheels and body acceleration transducers. These models have been modified to accommodate additional forces due to aerodynamic effects.

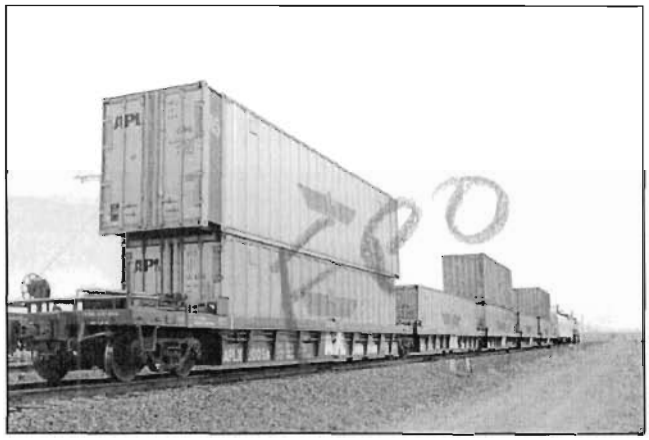

(a) 5-car consist

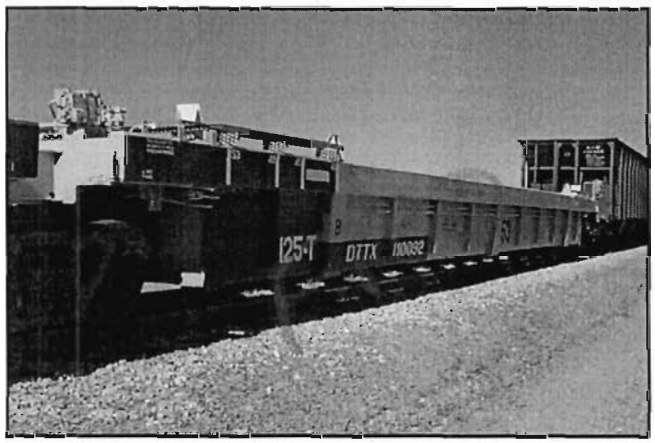

(b) Container car

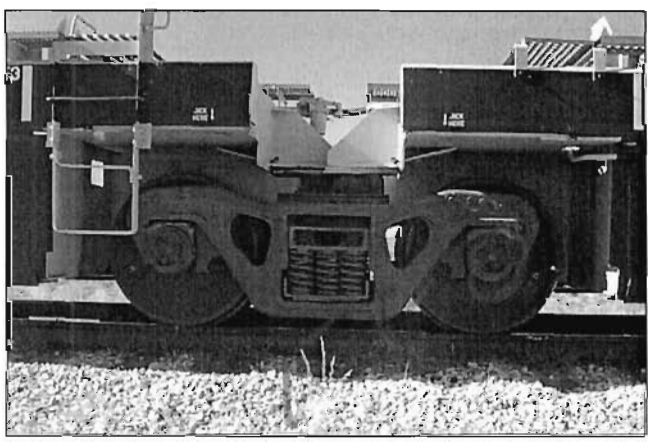

(c) Shared truck

Figure 15. Container Cars

For this study, NUCARS (Version 2.2) modeling was used to predict wheel/rail contact forces and general vehicle body motion as a means to assess dynamic stability and safety. A number of specific criteria were used to assess stability and safety including vertical wheel loading, the ratio of lateral to vertical wheel loads, wheel to rail contact angle, and general body motions of the car. According to the *Manual of Standards and Recommended Practices* of the Association of American Railroads, lateral to vertical wheel load ratios of 1.0 or higher, given a wheel angle of attack that is less than 5 milliradian, is the upper limit for safety as defined for specified controlled dynamic test scenarios. Dynamic vertical wheel loading at the rail that is less than 10 percent of static wheel loads occurring for 50 milliseconds or longer is also unacceptable. The degree of safety was assessed using these criteria. Wheel unloading and high lateral loads or large wheel to rail angle of attack can be precursors to increased risk of derailment and were therefore analyzed as part of this study. Additionally, whole body dynamic behavior characterized by roll, yaw, and pitch motions were used to evaluate car body envelope variations and general car-to-car dynamic displacements.

Computational fluid dynamics models are used to predict the aerodynamic loads, which are then supplied as input files to the NUCARS model. NUCARS reads the aerodynamic forces and moments utilizing these files as look-up tables of discrete values. The NUCARS integration time step is normally set at 0.025 milliseconds to maintain integration stability, while output samples from aerodynamic predictions contained in the look-up table are temporally spaced at 5 millisecond intervals, thus requiring linear interpolation between points. Figure 8, shows an example plot of the aerodynamic loads resulting from a high-speed pass between the Acela Express and a single car of a freight consist. The data in these look-up files provides resultant forces and moments referenced to the car body at rail height, centered between rails. This selected reference taken at rail height, which is essentially ground height, is the customary output format for CFD simulations. As a simplification, longitudinal and vertical forces were ignored because of their small magnitude and limited effect on dynamic behavior, which left the remaining lateral force and the three moment vectors (M_X, M_Y, M_Z). NUCARS calculates the resulting orthogonal load vectors at the wheel and rail interface, as well as resulting vehicle body dynamic displacements and accelerations. The aerodynamic input pulse provided by the CFD computations which was delineated in the look-up table, was used in the NUCARS model by sequentially replicating it for each car along the consist length spaced at the appropriate time interval for the passing Acela Express. It was shown in an earlier section that this simplification over full-consist aerodynamic modeling, which uses all the cars in a 5-pack consist, was within the range of predictive accuracy. Finally, the track model used for these analyses represents ideal conditions. Track variations in cross-level and gauge were not considered, but it can be expected that inclusion of such perturbations may further influence car dynamic stability.

The specific train configuration selected for analyses was a 5-pack (5-car) articulated double-stack container freight consist. The 5-pack double-stack consist as shown in Figure 15, was chosen because intermediate cars share single trucks. Shared trucks connect two cars and support half the weight of each neighboring car. Laterally located side contact bearings and a center plate on the truck, work to support pairs of cars both vertically and laterally. These joints act to transmit forces and moments between cars, thus providing a more direct dynamic link over other freight car designs using independent-coupler connected "unshared" trucks of non-articulated design. This dynamic link between cars of shared trucks can lead to accentuated movement with a resulting increase in the likelihood of instability or derailment. The freight consist was modeled using two levels of containers. The lower level consisted of two adjacent

20-ft long containers, while the top level consisted of one 53-ft long container, which is the maximum length allowed. Figure 16 shows schematic diagrams of the freight double-stack container consist relative to a passing high-speed train in both coincident and opposing directions. Specific modeling parameters such as car dimensions and inertial values used in the dynamic simulation are given in Table 2.

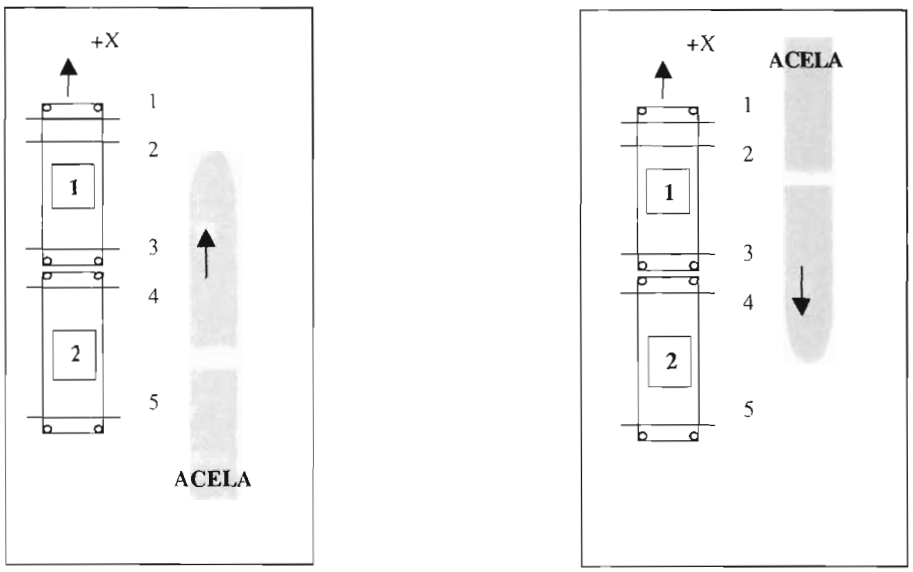

(a) Coincident (b) Opposing

Figure 16. Schematic of Acela Express and Freight Showing Axle Numbering

Table 2. Freight Car Modeling Parameters

	Length Between Bolsters in./(m)	Mass of Car Body without Trucks, with Empty / Fully Loaded Containers lbm/(kg)	Car Center of Gravity Height from Top of Rail for Empty/Fully Loaded Containers in./(m)	Roll, Pitch and Yaw Inertia for Empty / Loaded Containers lbf-in-sec^2 /(kg-m^2)
Double-Stack Freight car	708 (18)	47,257 (21,420) 134,980 (61,243)	71.1 (1.81) 68.8 (1.75)	9.8E5 4.9E6 4.6E6 (1.1E5) (5.5E5) (5.2E5) 1.46E6 8.27E6 7.71E6 (1.6E5) (0.93E5) (8.7E5)

2.4 DYNAMIC ANALYSIS - LOAD CHARACTERISTICS AND GROUPS

The train operating scenarios were divided into three groups to investigate the full range of response behaviors: maximum lateral force, maximum lateral impulse, and aerodynamic load timing. Consideration was also given to ambient wind vector as a modeling parameter. These load groups are described as follows:

1) Maximum change in lateral force - These cases are associated with a high-speed pass between trains operating in opposite directions. As expected, a peak load occurs with an Acela Express headwind (Case 5: see Figure 11), characterized by a short duration pulse. Similar peak conditions might also occur from a combination of a peak lateral crosswind velocity and negative pressure gradients developed at the trailing end of the high-speed train, with trains passing at high-speed in opposing directions.

2) Maximum lateral impulse - These cases, specifically 7 and 8, tend to occur when both trains are operating in the same direction, and the high-speed train is overtaking the slower freight consist, as depicted in Figure16(a). Although the peak aerodynamic load magnitude is normally less than that of load-group 1 for comparable wind conditions, the effective contact time is extended significantly. This extended contact time can bring the aerodynamic load pulse within the frequency range in which the consist would react to a rigid body vibration mode. This frequency would be within the bandwidth or time constant of the consist transfer function, thus transmitting the load without significant attenuation. Aerodynamic pulses that act on a much shorter time scale are attenuated because of the mass-filtering effect of the consist, its single degree of freedom time constant, thus minimizing the dynamic effect of the aerodynamic load.

3) Load timing or synchronized resonance loading - That portion of the cyclic part of the aerodynamic load for the cases discussed here, corresponds to the period associated with consist roll and yaw natural modes. By matching train closing speed to resonant modes of the consist, larger body movements may result. In these cases, the consist dynamic transfer function accentuates the input aerodynamic loads. Although the input peak aerodynamic magnitude may be smaller than the large peaks noted in load-groups 1 or 2, resonance accentuates or amplifies the input load and further causes the establishment of natural modes of vibration. Consist resonant frequencies in roll and yaw appear at train closing speeds between 100 mph and 130 mph. These resonant frequencies can be seen in Cases 10, 11, 12, 13, 15, and they also can be seen to some degree in Case 8.

All the above cases include variations in wind speed, wind direction, and vehicle closing speeds as shown in Table 1.

2.4.1 DYNAMIC ANALYSIS RESULTS - SUMMARY

Simulations were performed for the freight car consist under the three general load groups as mentioned earlier, and are restated here: (1) peak aerodynamic force and moment, (2) maximum aerodynamic impulse, and (3) synchronized car-to-car resonance loading. Most of the loading scenarios that were investigated used double-stack container cars carrying empty containers as worst-case representations. Lightly loaded cars are generally more likely to experience wheel unloading and large lateral to vertical wheel load ratios, which act to increase the risk of

derailment. Two other cases were examined that included partially loaded and fully loaded containers. In all the cases, the cars carried double-stack containers that were either empty or full as depicted by the lead car in Figure 15. Regardless of weight, each case represents the same aerodynamic surface area.

A matrix of NUCARS analyses for the freight consist was generated to quantify the effect of aerodynamic loads. Here, it should be noted that the range of operating conditions is considered a worst-case list of possible scenarios, which may not represent normal operating conditions. The extent to which results from these analyses predict derailment depends on the statistical likelihood of conditions occurring in such combinations. One worst-case combination would be a 50 mph headwind condition, combined with the high operating speed of the Acela Express as it overtakes a slower moving consist carrying empty double-stack containers. However, this combination of events may be relatively unlikely.

Wheel unloading and lateral to vertical wheel load ratio, as well as general rigid body dynamic behavior such as roll or yaw motion, were used to assess the likelihood of derailment. These criteria were used to show that the empty container consist subjected to aerodynamic loads had the greatest potential for derailment, as shown in Cases 8, 9,12 and 15 as shown in Table 1. Wheel unloading was extensive, occurring over a duration of 1.0 seconds in some cases. Cases 8 and 15 show the largest impulse, while Cases 12, 13, and 15 excite consist resonant modes. Cases 9 and 14 examine worst-case loading caused by a crosswind, coupled with negative wind loads generated at the end of the high-speed train. These last two cases produce serious container consist motions. The largest peak aerodynamic load noted in Cases 5 and 6 produced less severe dynamic behavior. Although this peak load was large it was sufficiently small in duration as it was out of the frequency response range of the car or consist, and little dynamic response was therefore noted. Such high loads could be significant, however, in the analyses of container attachment integrity or passenger window loads. The issue of window loads will be discussed in Section 3.

Similar analyses using partially loaded and fully loaded double-stack container cars showed improvement in dynamic stability. When all containers within the consist were fully loaded, wheel lift was eliminated and wheel L/V ratios remained below 1.0 for all cases except Case 9. Consists like the one shown in Figure 1, in which the first and last cars were fully loaded, but the other cars carried empty containers, continued to show some signs of wheel lift, albeit minor and very brief in duration. Upon examination of car body dynamic behavior, it was determined that roll motion is slight for all cases considered. Therefore, vehicle weight is the most important parameter affecting wheel unloading. Wheel unloading is more a result of lateral motion than car body roll. What this means is, that uneven container loading from top to bottom, which has an effect on roll inertia, has less influence than the overall weight of the car. This finding is a result of the aerodynamic loads occurring at or near the same elevations as the car body's center of gravity, whether the containers are loaded or not.

A summary of case study results showing the cases and conditions that failed to meet chapter XI specifications of the AAR standards are outlined in Table 3. The table specifically defines the minimum wheel loading, and maximum L/V ratio for those conditions that failed. According to chapter XI of the AAR standards, failure can occur for either a dynamic wheel load that falls below 10 percent of the static wheel load for 50 milliseconds, or failure can occur when the ratio of lateral to vertical load exceeds 1.0 for 50 milliseconds. The table defines conditions of

loading for either empty, partially or fully loaded cars that produced unacceptable results for each failure case. Details of these cases are discussed in the following section.

2.4.2 DYNAMIC ANALYSES

For each aerodynamic load, the container consist response was evaluated by simulating consists with all empty containers as well as consists with a combination of loaded and empty containers. In the case of partially loaded consists, conditions were examined where the first and last cars were loaded and the central cars were empty, in order to understand the extremes of load configurations. Detailed results of this study are discussed in the following paragraphs.

Table 3. Summary of Case Performance Measured Against AAR Chapter XI Specifications

Cases*	Minimum % Wheel Load** (P = pass, F = fail)	Maximum L/V*** (P = pass, F = fail)
1	P	P
2	P	P
3	P	P
4	P	P
5	P (Near Failure with Empty Containers) Truck-1 (16%), Truck-6 (61%)	P Truck-1 (0.0251), Truck-6 (0.0815)
6	P	P
7	P	P
8	F – Empty, P – Partially and Fully Loaded Truck-1 (5.7%, Truck-6 (53%)	P Truck-1 (0.08), Truck-6 (0.22)
9	F – Empty, Partially and Fully Loaded Empty and Partially: Truck-1 (0),Truck-6 (0) Loaded: Truck-1 (46%), Truck-6 (8%)	F – Empty and Partially, P – Fully Empty and Partially: >1 Loaded: Truck-1 (0.16), Truck-6 (0.068)
10	P	P
11	P	P
12	F – Empty, P – Partially and Fully Loaded Empty: Truck-1 (0), Truck-6 (30%) Partially: Truck-1 (27%), Truck-6 (61%) Fully: Truck-1 (55%), Truck-6 (78%)	F – Empty, P – Partially and Fully Loaded Empty: Truck-1 (>1), Truck-2 (0.15) Partially: Truck-1 (0.06), Truck-6 (-.07) Fully: Truck-1 (0.03), Truck-6 (0.03)
13	P	P
14	F – Empty, and Partially, P – Fully Empty: Truck-1 (0), Truck-6 (0) Partially: Truck-1 (4%), Truck-6 (34%)	F – Empty, and Partially, P – Fully Empty and Partially (>1) Fully: Truck-1 (0.3), Truck-6 (0.46)
15	F – Empty, and Partially, P – Fully Empty: Truck-1 (0), Truck-6 (24%) Partially: Truck-1 (0), Truck-6 (58%) Fully: Truck-1 (31%), Truck-6 (76%)	F – Empty and Partially, P – Fully Empty and Partially (>1) Fully: Truck-1 (0.04), Truck-6 (0.03)

* Pass or Fail as noted by container loading: Empty, Partially and Fully
** Minimum vertical wheel load not to be less than 10% of static wheel load for 50 msec.
*** Maximum ratio of wheel lateral to vertical load not to be greater than 1.0 for 50 msec.

Load Group 1: Maximum Change in Lateral Force

Peak changes in lateral force are seen in Cases 1 through 6 where the trains are operating in opposite directions. The idea of a change in load is introduced here to distinguish these cases from those with a steady crosswind where the lateral force may have a large static component. The more severe motions were predicted to occur when these loads are applied to a freight consist carrying empty containers. The largest peak load of Load Group 1 occurred for Case 5 in which the high-speed train passed (approached) the freight train at a closing speed of 200 mph. An ambient wind speed of 50 mph acted against the forward motion of the Acela Express train. Although this combination of train and wind speeds may produce the largest change in aerodynamic load, it does not represent the worst-case for dynamic stability, as will be shown. Figures 17 through 20 show plots of freight car vertical and lateral wheel forces, and car-body roll motion for the worst performing car or truck of the consist. Figures 17 and 18 show forces for the lead axle of Car 1, which passes Acela Express first. Figure 19 shows the vertical wheel forces of Car 5, the last car to pass the Acela Express. Figure 20 shows the roll motions of all five cars in the train consist. Based upon examination of the wheel loads and roll motions of Case 5 and other cases of Load Group 1, it is believed that the cases of this group are generally benign.

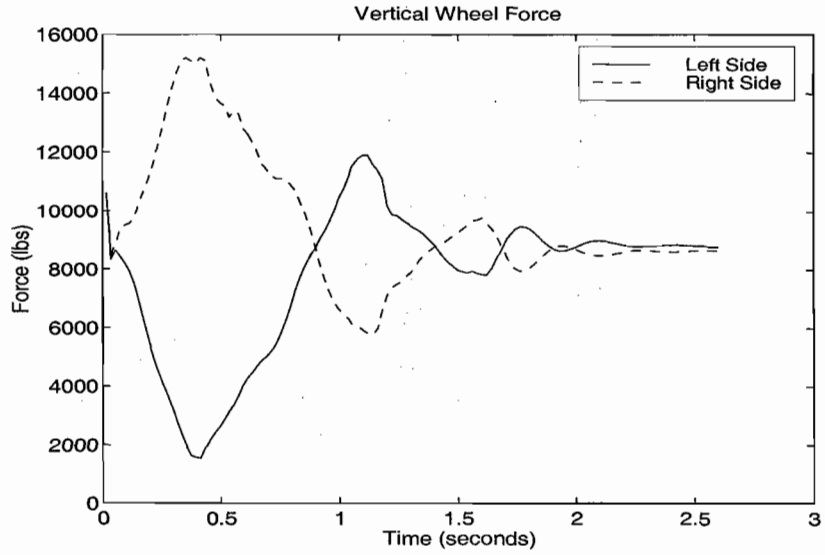

Figure 17. Vertical Wheel Force (Case 5, Axle 1)

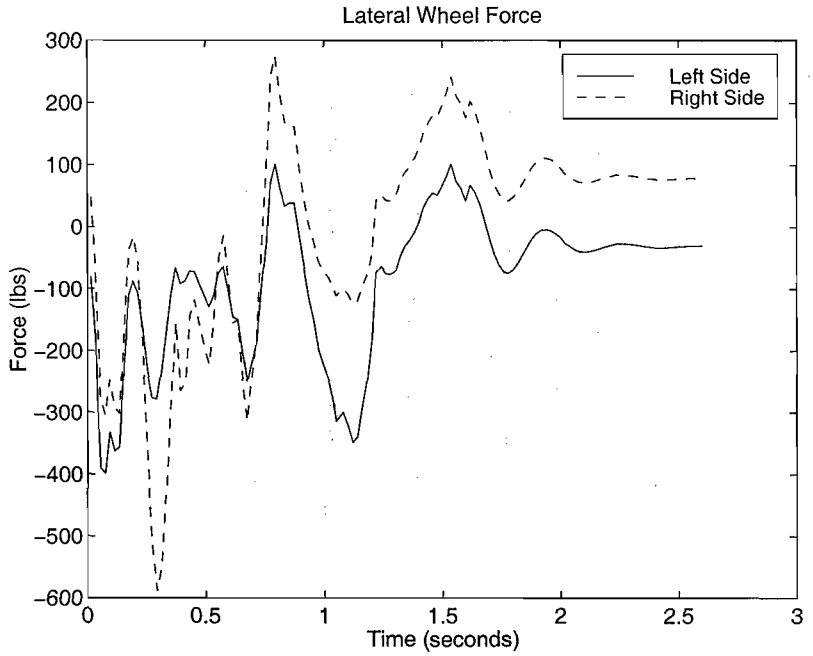

Figure 18. Lateral Wheel Force (Case 5, Axle 1)

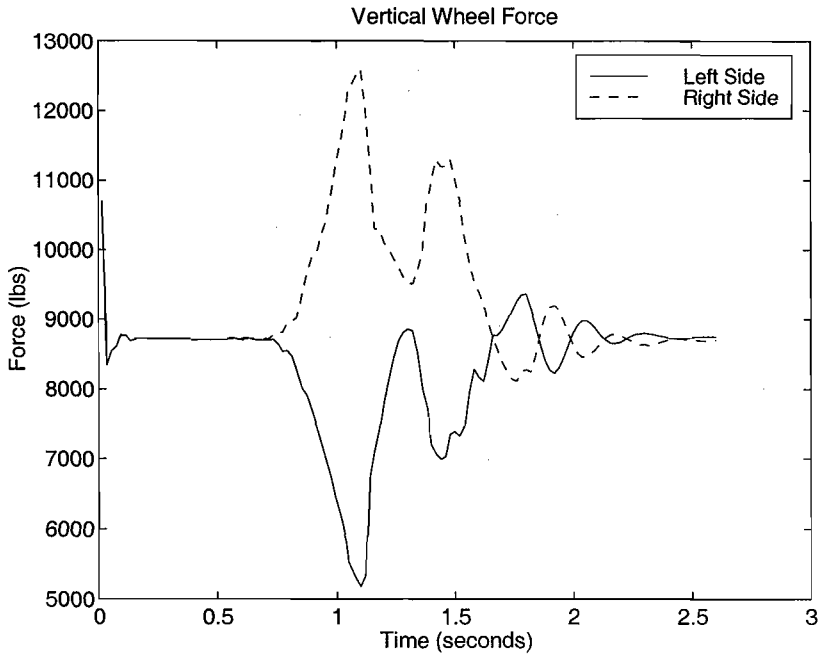

Figure 19. Vertical Wheel Force (Case 5, Axle 12)

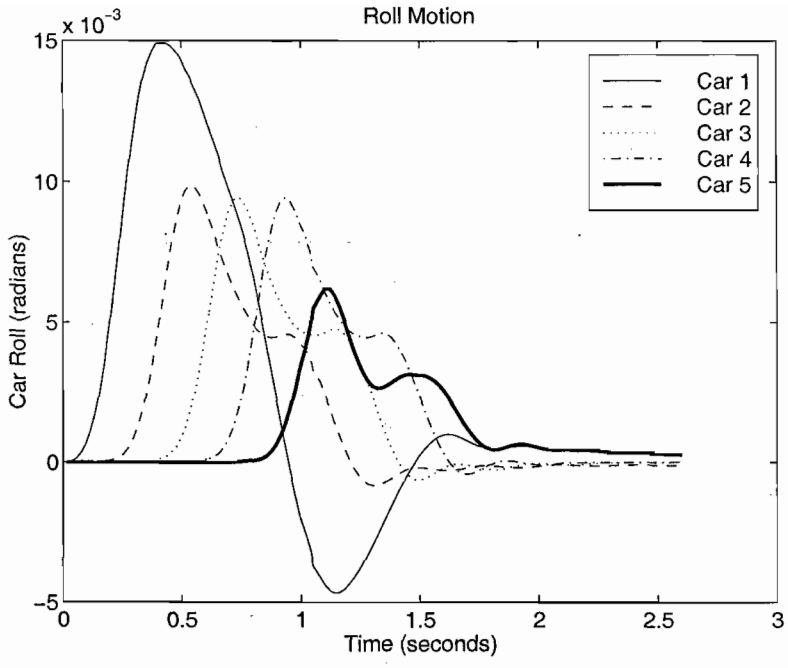

Figure 20. Car Body Roll Motion (Case 5)

Load Group 2: Maximum Lateral Impulse

The largest lateral aerodynamic impulse is seen in Case 8. In this example, an Acela Express operating at a speed of 150 mph overtakes a freight consist traveling at 50 mph, resulting in a closing speed of 100 mph. The ambient wind velocity opposing both trains is 50 mph. A comparison of the lateral impulses for several cases given earlier in Figure 14, shows a wide variation in impulse with operating conditions. The lateral impulse of Case 8 measured in units of Newton-seconds is 8410, or about twice that seen in Case 5. For this worst-case condition, the freight car roll and yaw motions between adjacent cars is generally out of phase, with some indication of an increase in roll and yaw amplitude from the first car encountered by Acela Express (Car 5) to the last (Car 1). Figures 21 and 22 show the roll and yaw motion of each freight car in the train consist. In these figures, Car 5 reacts first as Acela Express overtakes the container train from the rear beginning at Car 5, with Car 1 at the opposite end of the train. The largest roll motion is seen in Car 1. Both the lead (consist car number 1) and trail (consist car number 5) cars can be expected to behave differently from intermediate cars within the consist, as the end trucks of these cars do not share the weight of two car ends and are therefore more lightly loaded. The ends of these cars can be expected to have larger dynamic motions and a greater risk for wheel unloading. The other cases mentioned in this study also reveal that the end cars experience the greatest safety risk

Lateral displacement of each car's center of gravity is shown in Figure 23, where it is noted that Cars 1 and 5 have the largest displacements. Upon closer examination of the vertical wheel loads of Car 1, Axle 1 (Figure 24), the vertical force of the right wheel nearest the Acela Express approaches zero, and corresponds to the point of maximum lateral car body load shift which occurs at a time of 2.7 seconds. This trend is noted for both Figures 23 and 24. It is clear that

load shifting between left and right wheels is generally 180 degrees out of phase indicating a rocking or shifting in lateral load. Figure 25 depicts lateral wheel force. Dynamic vertical wheel loading reaches a minimum of 505 lbs. When compared to a static wheel load of 8,720 lbs, the wheel loading is only 5.7 percent, which clearly exceeds AAR standards.

Except for Car 1, the other cars in the freight consist experiencing this same loading environment did not show dynamic reactions, which required immediate attention. There is evidence of anti-symmetric rocking and lateral shifting of the cars, however, minimum vertical wheel loads are greater than 6,000 pounds. Figure 26 shows the variation in vertical wheel force of Axle 3, the lead axle of the second truck. The ratio of dynamic to static wheel loads in this case, using a static wheel load of 13,700 lbs, resulted in a 47 percent wheel loading, which is well within AAR standards. Lateral loads were minimal and the ratio of lateral to vertical loads was less than 0.5.

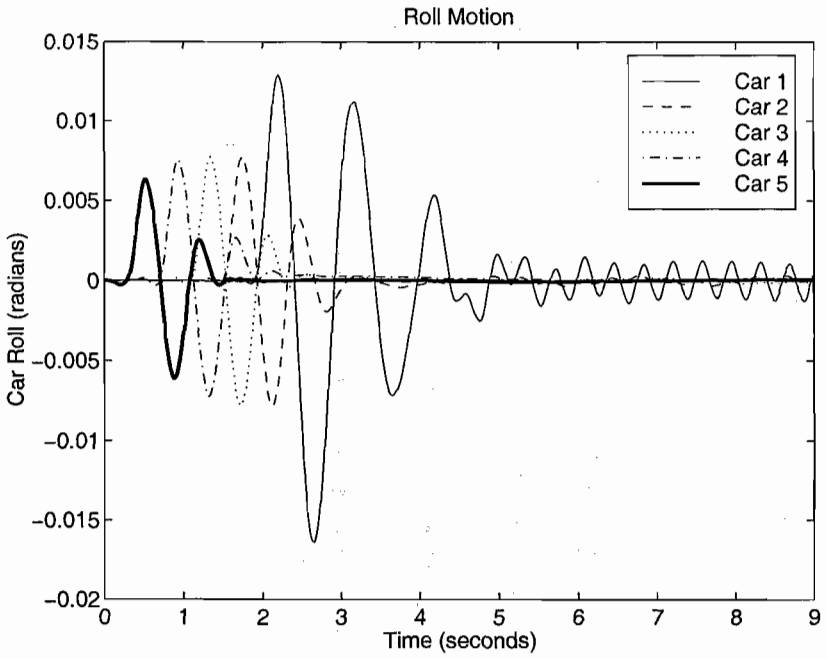

Figure 21. Car Body Roll Motion (Case 8)

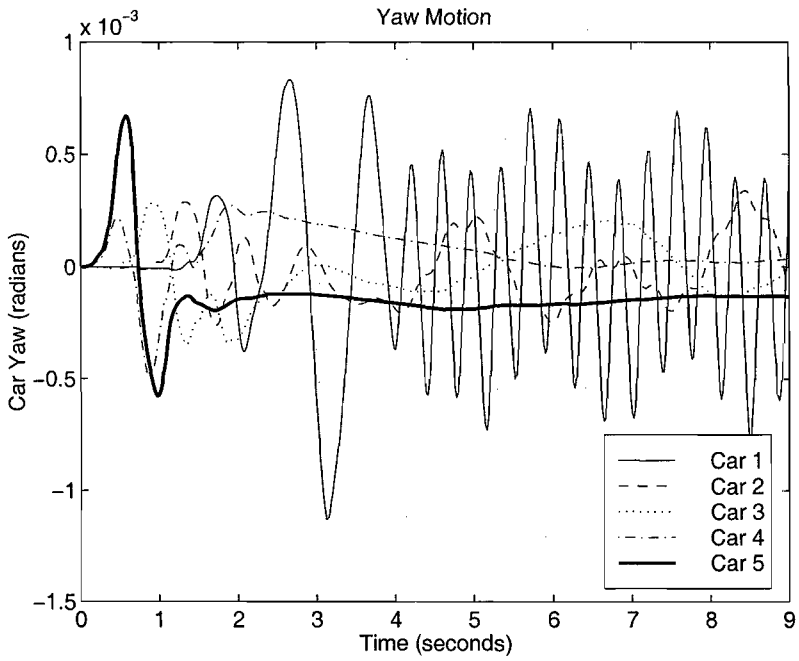

Figure 22. Car Body Yaw Motion (Case 8)

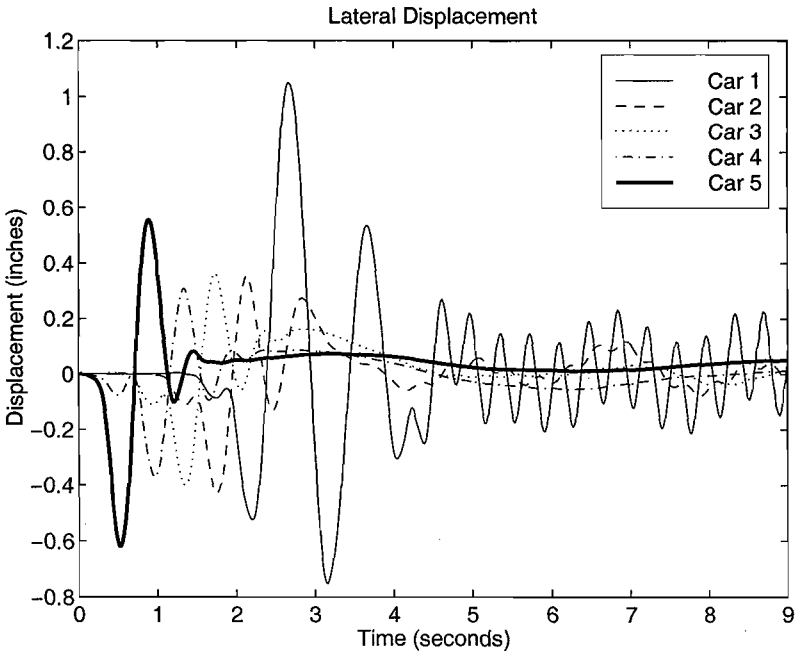

Figure 23. Car Body Lateral Displacement (Case 8)

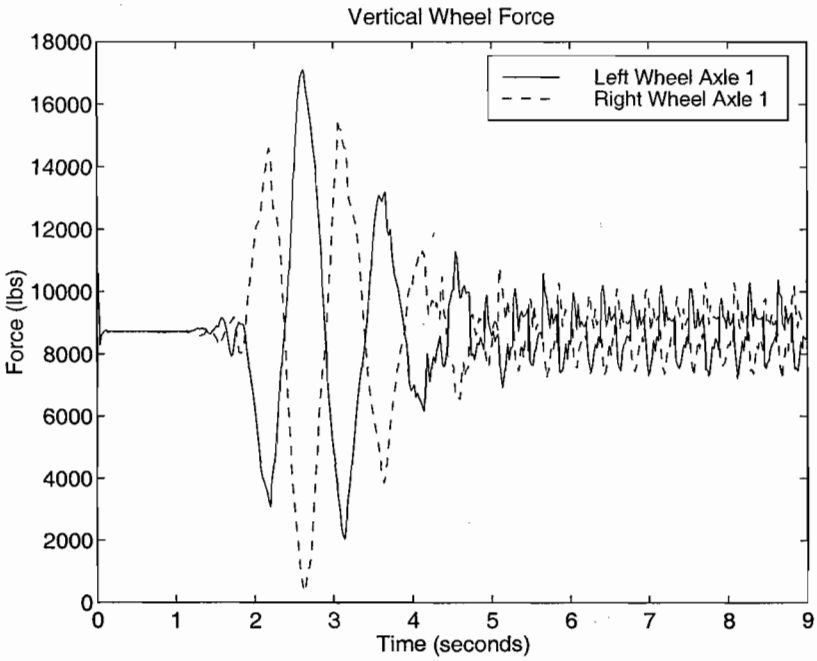

Figure 24. Vertical Wheel Force (Axle 1, Case 8)

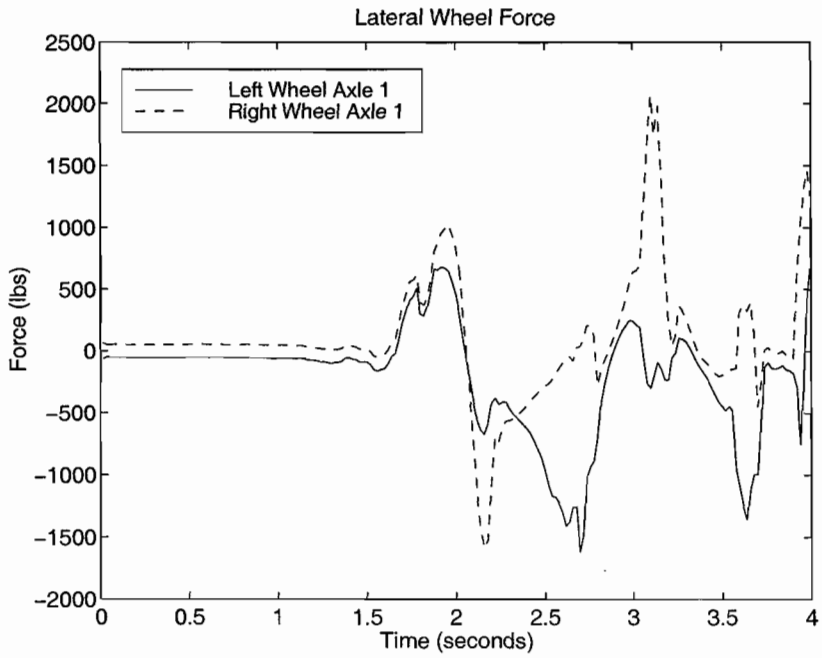

Figure 25. Lateral Wheel Force (Axle 1, Case 8)

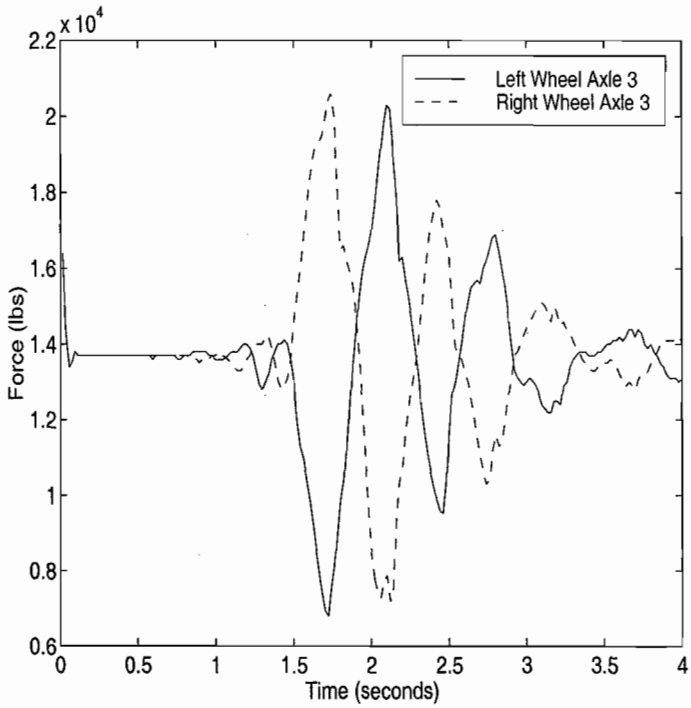

Figure 26. Vertical Wheel Force (Axle 3, Case 8)

Load Group 3: Phased Loading Periods

Synchronization of the aerodynamic loading with consist rigid-body vibration modes is seen in Cases 10 through 13, and in Case 15. This effect is also seen to some degree in Case 8. The load periods in these cases bracket the expected consist lateral resonant mode periods. Analyses revealed that these lateral vibration modes have a temporal period of approximately 0.20 seconds, in relation to a closing train speed of approximately 130 mph, with a car length of approximately 60 ft. The NUCARS analyses show that Case 12 at a closing speed of 120 mph, and Case 15 with a closing speed of only 70 mph produce the highest magnitude and duration of wheel unloading and are the most severe of the cases analyzed in this study. These cases have been focused on for the purpose of this study.

The consist response for Case 12 is illustrated in Figures 27 and 28, which depict vertical wheel forces for the first and third axle in the consist, respectively. Note again, the cyclic nature of wheel unloading. Large amplitude fluctuations are observed when the Acela Express reaches the first car at a time of 1.7 seconds. The Acela Express is completely past the freight consist at a time greater than 2.5 seconds, after which the consist continues its large amplitude cyclic wheel unloading behavior. (Computation of these times is based on a consist length of approximately 350 ft, a car length of approximately 60 ft, and a closing speed of 120 mph.)

Figure 28 shows the vertical wheel load of Axle 3, which is in Truck 2 of the first car. Note the similarity between the response of Axle 3 and that of Axle 1 in the first truck. The reason Truck 1 experiences more unloading is the first truck is not shared, and therefore is lightly loaded. The

first truck also has a standard coupler at its end, while the second truck is connected using an articulated connection. For both axles, wheel unloading violates AAR standards for safety.

Case 15 shows the longest duration of wheel unloading. For this case, the closing speed of the freight consist is 70 mph, while the Acela Express operates at a speed of 120 mph. The increased risk of this case may have initially been counterintuitive, because it may have been expected that if the two trains passed each other at slower speeds, dynamic interaction would be less. However, the natural response of the consist accentuates the effect of the aerodynamic loads. Figures 29 and 30 show the vertical wheel force for the first and third axles, respectively. In this case, wheel unloading for both left and right sides of Axle 1 become zero, showing the familiar load rocking behavior. From Figure 31 it can be seen that lateral wheel displacement of Axle 1 produces flange contact with the rail. The computed consist dynamical behavior is certainly severe, but it must be remembered that all of the double-stacked containers being carried by each car are empty.

Operating the freight consist while using only empty containers, shows a high level of dynamic response, especially for Case 15. Perhaps a more commonly used configuration is to partially load some of the containers or fully load all of the containers. This was done using the operating conditions for Cases 8, 12, and 15. Two additional NUCARS analyses for each of these cases were run in order to determine the sensitivity of dynamical behavior to car weight. One case used partially loaded containers (75 percent of maximum permissible) for the first and last car of the freight consist with all other cars empty. Another case used fully loaded containers for all cars. Partially loading the first and last cars is expected to aid in the reduction of wheel lift as the lead or trail trucks are lightly loaded. It is also expected that fully loading all of the container cars in the freight consist will reduce the risk of derailment because of the change in the dynamical characteristics of the load, as well as the change in weight.

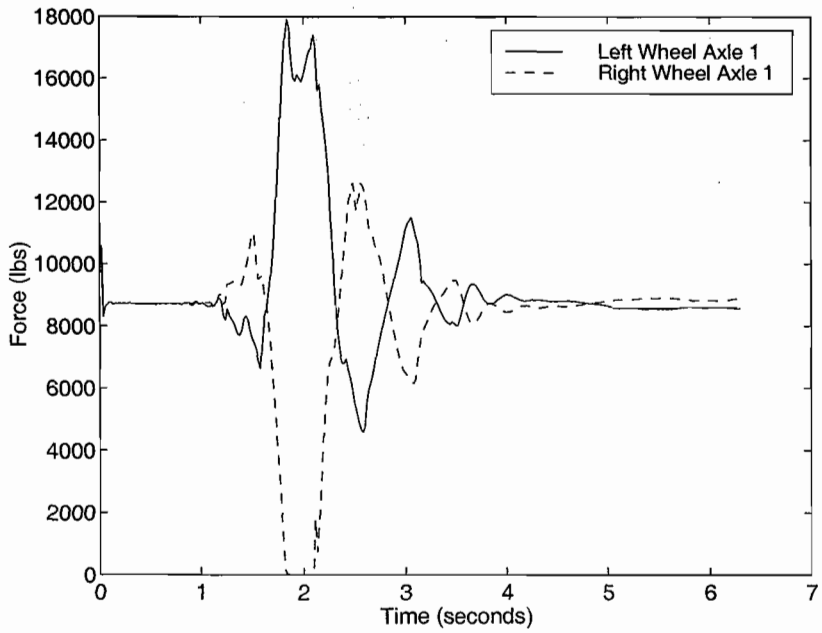

Figure 27. Vertical Wheel Force (Axle 1, Case 12)

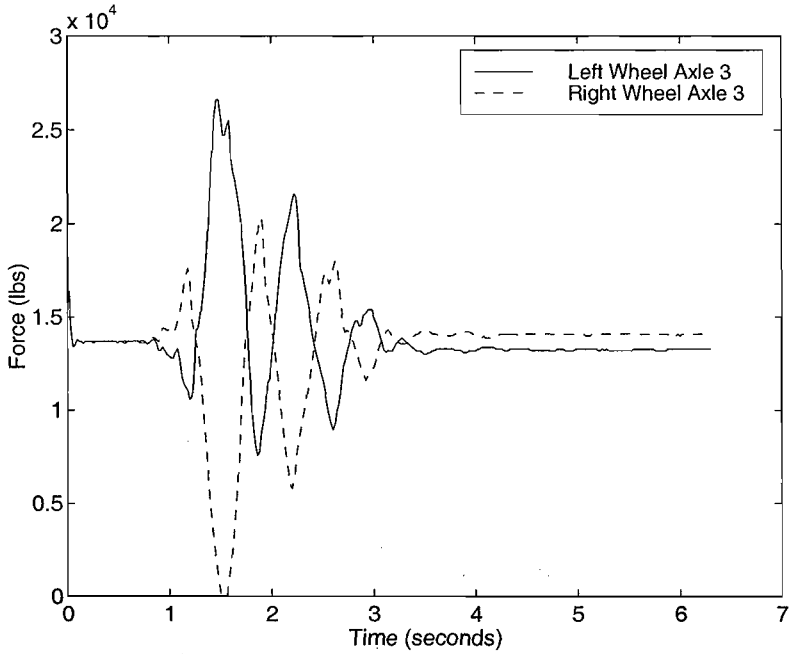

Figure 28. Vertical Wheel Force (Axle 3, Case 12)

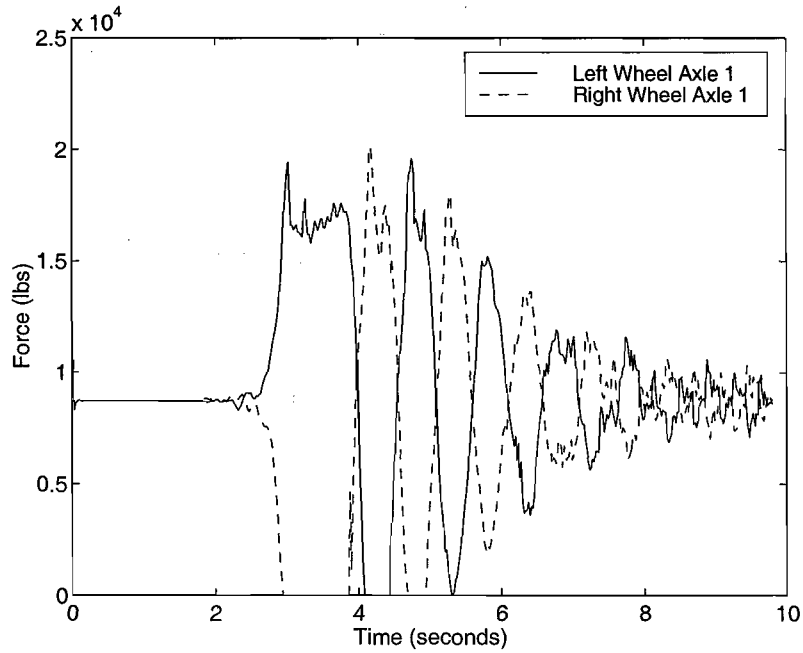

Figure 29. Vertical Wheel Force (Axle 1, Case 15)

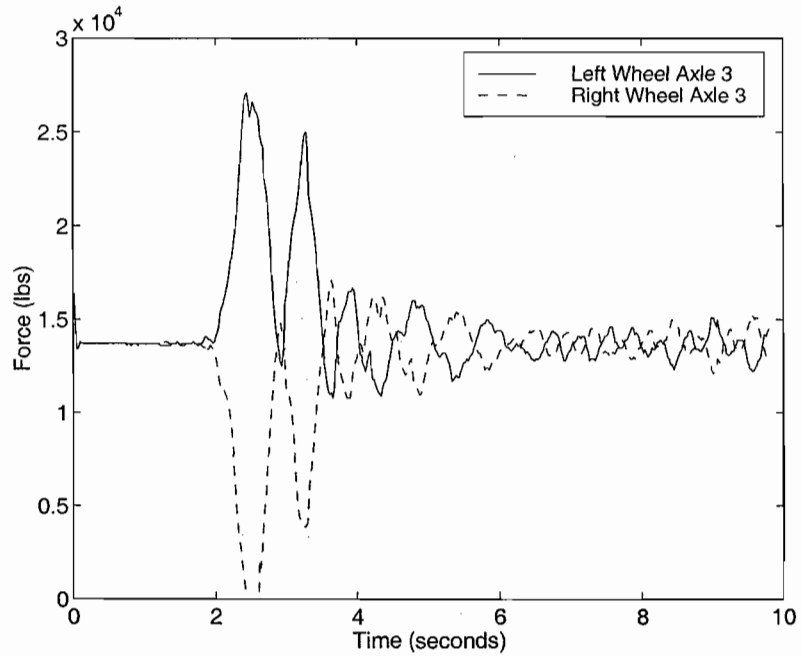

Figure 30. Vertical Wheel Force (Axle 3, Case 15)

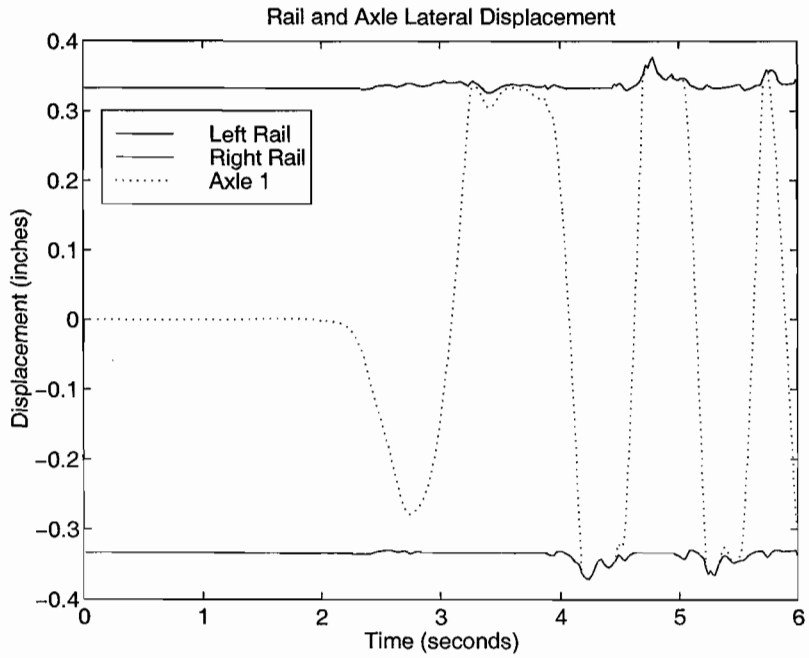

Figure 31. Lateral Axle Displacement (Axle 1, Case 15)

When all the containers in a freight consist are fully loaded, the problem of dynamical instability disappears. Vertical load on the right side of Axle 1 is seen to exhibit the common load-rocking behavior, but the amplitudes are significantly smaller. Vertical wheel forces are never less than 10 percent of the static wheel load. For the partially loaded case like that seen in Case 15, the risk of derailment still remains. The vertical wheel forces of Axle 1 dropped to less than 10 percent of the static wheel load, which is an unacceptable level.

The last cases analyzed examined the effects of crosswind coupled with the transient aerodynamic loads from the two passing trains. This combination of loads also leads to potentially serious effects for unloaded container car configurations, as seen in Cases 9 and 14. Here, the wind velocity vector is in a negative Y direction, or from the freight consist track towards the Acela Express track. Added to this lateral wind pressure load is a lateral dynamic load in the same direction produced when the back-end of Acela Express passes the freight consist. Computer simulations of these cases using all empty containers failed to produce results for long integration times as a result of convergence problems that occurred when the wheel loads of the freight consist became zero (fully unloaded), and the wheels further separated from the track. It is speculation as to what dynamic behavior is actually occurring at times beyond this large wheel-to-rail displacement, but it can be expected that for empty container consists, these large lateral aerodynamic loads can produce significant wheel unloading

When all the container cars were fully loaded as seen in Cases 9 and 14, the computer simulation successfully completed and demonstrated acceptable dynamic behavior, without a risk of derailment. However, this was only achieved for Case 14. Case 9 still had an unacceptable wheel unload of 8 percent, which occurred at the last car. When only the first and last cars carry partially loaded containers, there remains a risk of excessive wheel lift and potential derailment for both Cases 9 and 14.

2.4.3 DYNAMIC ANALYSES – CONCLUSION

In conclusion, there are operating conditions of the 5-car articulated double-stack container consist that are likely to have unacceptable dynamical behavior that exceed AAR safety standards as identified for specific controlled dynamic test scenarios. In general, given ambient wind speeds of 50 mph, consists carrying empty double-stack containers show detrimental wheel unloading. Potential problems may arise when freight consists are passed by high-speed trains like the Acela Express, even when closing speeds are as low as 70 mph. It was shown that these lower closing speeds produce more serious effects than much higher closing speeds in either coincident or opposing directions, given an Acela Express speed of 120 mph. Acceptable performance is obtained for all except Case 9, when all containers are fully loaded. When only the lead and trail cars of the consist are loaded to 75 percent of the maximum container weight, serious wheel unloading for Cases 9, 12, 14, and 15 occurred.

3. CONTAINER DISLODGEMENT AND WINDOW BLOWOUT

Container Dislodgement – In addition to examining the issue of derailment, the question of container dislodgement was also examined. The maximum lateral and vertical loads on the top containers were calculated and compared to the strengths of the tie-downs. Peak vertical loads on the container alone were observed to be on the order of 12,000 N, or on the order of 3,000 lbf. This is less than the unloaded container weight, so the vertical load on the tie-down is zero, and *the upper container is supported by the lower one. The maximum lateral forces were considerably more, about 5,600 lbf or 25,000 N. Specification for tie-down strengths seems to emphasize resistance to axial and vertical loads rather than transverse loads. Specifically, the tie-downs must be able to handle a weight greater than that of the gross container weight. Tie-downs should be able to accommodate twice the loaded weight in the axial and vertical directions, and 0.3 times the container weight in the transverse direction. The maximum loaded weight rating of 20-ft containers is 52,900 lbf (235,000 N), and the maximum MGWR of containers over 20 ft is 67,200 lbf (299,000 N). Table 4 compares the tie-down strength with the aerodynamic loads on the container. As shown in Table 4, properly tied down containers should not become dislodged.

Table 4. Comparison of Tie-Down Strength with Load on Containers

	20 foot Container		Greater than 20 feet	
Load Direction	Tie-down specified strength (lbf)	Peak Aerodynamic Load (lbf)	Tie-down specified strength (lbf)	Peak Aerodynamic Load (lbf)
Axial	105,800	3,000	134,400	3,000
Vertical	105,800	0	134,400	0
Transverse	15,870	5,600	20,160	5,800

Passenger Car Window Blowout – Special runs were made to determine window loads on a bi-level commuter car when passed by Acela Express. These calculations were made using a revised mesh in which the bi-level commuter-consist was modeled as a long unbroken contour. By specifying the flow velocity and bi-level commuter surface velocities with respect to Acela Express, this dilemma is reduced to a steady flow problem rather than a dynamic problem. The tacit assumption here is that no special problems exist during the aerodynamic interaction at the extreme ends of the bi-level commuter consist. This assumption seems reasonable since experience with the container car calculations suggests that the maximum pressure amplitude on the side of the car remains relatively constant during the passing sequence. Figure 32 shows pressure contours on the Acela Express and the bi-level commuter consist with Acela Express traveling at 150 mph. The resultant pressure on the side of the bi-level commuter train at the lower window height is shown in Figure 33.

By examining Figure 33, it is possible to observe that the maximum pressure amplitude on the window is about 0.12 psi (18 lb/ft^2). Calculations on varying Acela Express speed revealed that the pressure amplitude varies as the square of Acela Express velocity, so that the maximum load will occur when Acela Express is facing a headwind.

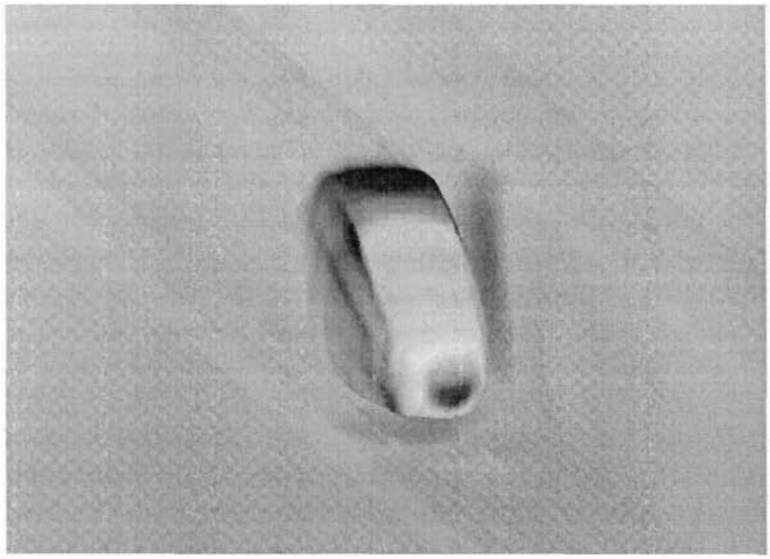

Figure 32. Pressure Contours on Acela Express and Bi-level Commuter Passenger Trains at 150 mph. Contour Range from –0.22 psi to 0.36 psi.

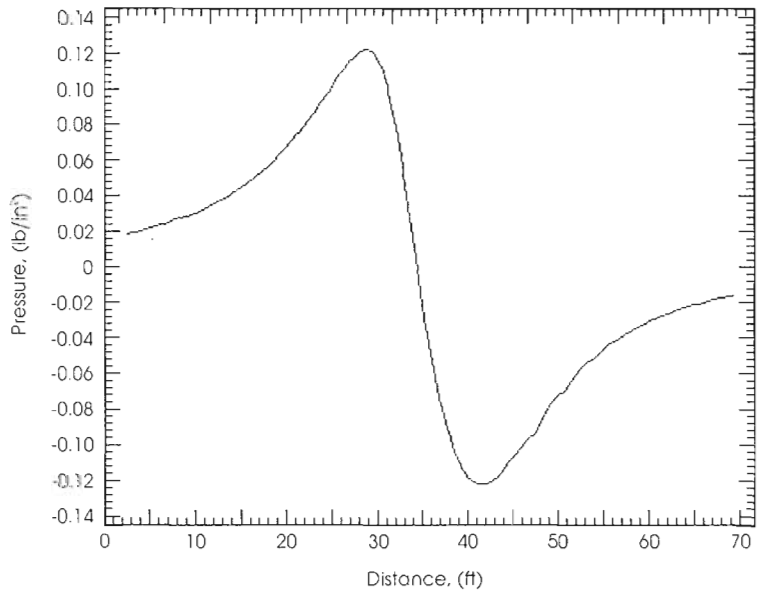

Figure 33. Pressure at Lower Window vs. Distance Along Cars at Lower Window Level.

Assuming the presence of a 50 mph headwind, the maximum pressure becomes (0.22 psi) 32 lb/ft^2. Drawings were not available of the windows on the bi-level commuter car, but some data was made available from recent impact tests conducted by the Volpe National Transportation Systems Center on similar windows.

The windows in the impact test had a total length of about 4 ft, and a height of about 2 ft (1.2m x 0.6 m). Thus, the maximum dynamic load on the entire window could reach 256 lbf (1,140 N), with a range of 512 lbf (2,280 N). It is also possible that the pressure inside the bi-level commuter car might be different from the ambient pressure, so that the loads could be even greater. The total force was integrated on the window with respect to time in order to get maximum total impulse. This resulted in a value of 14 lbf-s when the two trains were traveling in opposite directions, and 46 lbf-s when the trains were traveling in the same direction with Acela Express facing a 50 mph headwind (a worst-case).

The significance of the pressure loads on the windows of the bi-level commuter car is difficult to assess. Although the total forces seem significant, the predicted pressure fluctuations are not unusual for trains entering a tunnel. In the impact tests using steel balls mentioned above, the windows resisted an impulse level of 16 lbf-s successfully and it was assumed that this was a safe impulse level. Because the predicted impulse from the aerodynamic loads may be greater than the known safe impulse in some situations, i.e., when the two trains are traveling in the same direction against a strong headwind, it cannot be assumed that window breaking or blowout will not occur. A more detailed structural analysis of commuter train windows when passed by the Aclea Express train is needed in order to more accurately assess the risk of window blowout and breakage.

4. CONCLUSIONS AND RECOMMENDATIONS

Aerodynamic and vehicle response calculations have been combined to examine the dynamic safety implications of operating Acela Express on parallel track as it passes high profile double-stack container freight cars and high profile bi-level passenger commuter cars. Combinations of operating conditions and system configurations were selected to examine worst-case scenarios, such as ambient wind speeds of 50 mph, combined with selected train speeds and a track spacing of 12 ft. Intermediate cases that would not provide such a severe dynamic environment were not studied in detail, as it was the intent of the study to determine if worst-case conditions have safety implications. Further studies may be required to more precisely define dynamic characteristics associated with more common operating conditions.

The CFD calculations revealed that the greatest aerodynamic loads between trains occur when the front-end or the back-end of Acela Express passes the parallel train traveling on tangent track. Cars are subjected to a lateral push-pull force causing both rolling and yawing moments, and lateral car movement. It was found that the amplitude of the load depended the most on the Acela speed and the presence of a headwind. The load timing depends mostly on the closing velocity of the two trains. The presence of a crosswind can increase the absolute magnitude of the lateral load significantly but does not appear to increase the dynamic component of the load.

Three load characteristics were found to be important in studying container consist response: 1) the amplitude in lateral force, 2) maximum impulse, and 3) aerodynamic load timing, or simply the closing speed between trains. In the last case of aerodynamic load timing, aerodynamic loads that are in phase with consist resonance modes are the most severe. Passing train scenarios were chosen to study the effects of each of the three load characteristics. It was discovered that maximum impulse and load timing are more important than maximum lateral force in producing conditions that increase the risk of freight car derailment. Specific cases within these general categories were evaluated using empty and loaded containers, and analyzed for various ambient wind vectors and train speeds. Results revealed that serious risks may exist for articulated freight empty container cars, but conditions improve for consists containing partially and fully loaded containers. Some special cases were found that might cause derailment. In particular, the aerodynamic loads resulting from a crosswind in combination with the dynamic loads caused by the end of a passing Acela Express train cause complete wheel unloading for a period of nearly 1 second. Some improvement was found when the freight train carried all fully loaded containers, although there is still some risk of derailment for the cases studied.

The problem of container dislodgement was also examined. Based on current specified tie-down strengths for shipping containers, it does not appear that a properly restrained container would break loose under the conditions investigated in this study. However, it might be prudent to re-assess the required tie-down strength for lateral loads as an added safety margin.

The potential for passenger train window breakage or blowout that could occur when a commuter car is passed by Acela Express was examined using maximum predicted aerodynamic loads distributed across the window surface of a bi-level car. Total loads can reach 250 lbf (1,100N). In general, however, results of the examination were inconclusive. A more definitive assessment

of the risk of window damage or blowout will require a detailed structural analysis. This would include an assessment of the variability in window glazing strength and an assessment of effects due to window strength reduction from prior glass damage.

Finally, the authors believe that this study has revealed that Acela creates some potential risks to trains operating on adjacent tracks, especially for those trains operating under specific conditions. However, this study has not evaluated the degree of risk or the best methods for mitigating risk. Nor, has it addressed those scenarios where rare combinations of operating conditions may occur.

APPENDIX-A

DATA REDUCTION

The unsteady fluid flow models used in this study utilized the moving boundary condition to simulate the effect of the container car moving through the mesh. The container cars themselves were modeled using a fixed surface in the mesh as shown in Figure 2. The forces and moments on the container and car were obtained by integrating the pressures on the car and container surface over the region occupied by them. It was discovered that because the ends of the container did not always correspond to a node location in the mesh (where pressures are output), the resultant forces contained jitter or noise introduced by the data reduction procedure. Figure A-1 shows examples of the axial and transverse force resultants for Case 5 before and after smoothing. In this case, the container car is moving at 50 mph (22.35 m/s) with a 50 mph tailwind, so the steady drag on the container is low and the un-smoothed and smoothed curves look very similar. It was found that the roughness of the force and moment histories tended to increase with the amount of headwind on the container. Figure A-2 shows a more typical example taken from Case 10 where the container moves at 50 mph through still air. In this case, the drag force, and to a certain extent the transverse force, showed a significant amount of jitter introduced by the data reduction procedure. Thus, the need for smoothing becomes more apparent. It is important to note that most of the jitter in the force histories occurred at early and late times when the container was in the coarsest part of the mesh. The curves are smoother during the time of maximum interaction when the container is near the front of Acela. As applied here, the method acts as a low-pass filter, suppressing frequencies above 100 Hz.

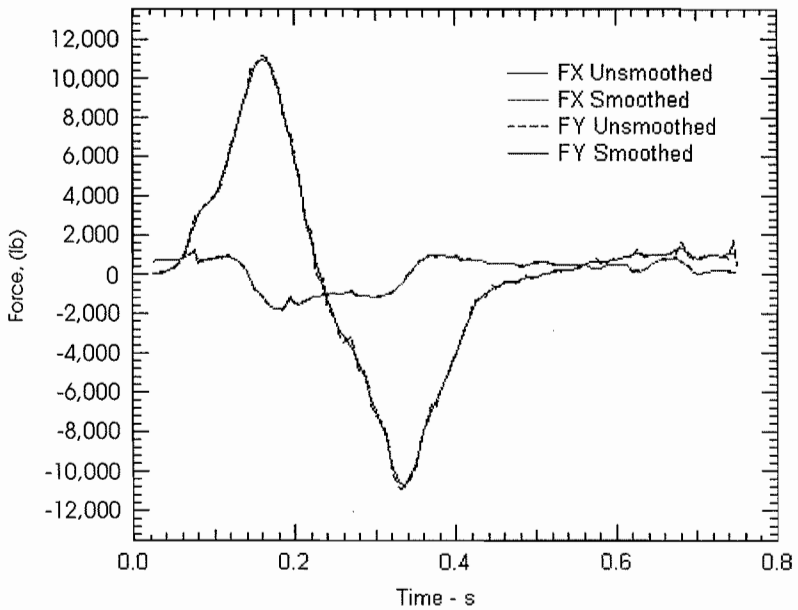

Figure A-1. Smoothed and Un-Smoothed Force Histories from Case 5

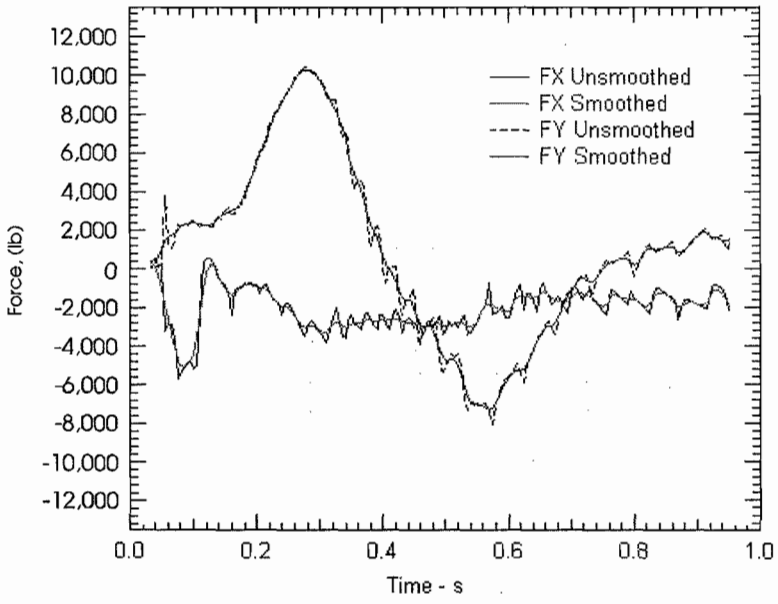

Figure A-2. Smoothed and Un-Smoothed Force Histories from Case 10

APPENDIX-B

VERIFICATION PROBLEM

This study used a novel method called the "moving boundary condition," to model the large relative motions of Acela Express and the container train. This method allows for the quick and efficient calculations of a body in motion without resorting to sliding fluid-fluid interfaces. Besides eliminating the overhead associated with interfaces, this method eliminates the potential for additional domain decomposition during the calculation. However, the use of this method does raise questions about accuracy. In order to give a sense of the potential loss in accuracy associated with the method, a special problem was devised that allows direct comparison of the force histories derived by the method used in this study, and those obtained from modeling with a fixed boundary in a mesh. In this example, two simple containers (rectangular parallelepipeds) were assumed to pass each other at 75 mph (33.5 m/s) in opposite directions, in still air. The sizes of the containers are the same as those in the passing train problem. One of the containers was modeled using a fixed surface in the finite element mesh, and the other was modeled using the moving boundary condition method. Thus, in the ideal case, the surface pressure contours on the containers will appear similar and the force resultants on the two containers would be equal and opposite. Figure B-1 shows surface pressure contours on the surface of the fixed box (left), and the moving boundary condition (right) for the test problem at a time when the two containers are partially past one another. The relative position of the containers can be most easily seen in the figure on the right where the fixed container is not rendered and a large black shadow appears at its location. Pressure contour lines on the ground around the container are also shown. Figure B-1 shows that the surface pressures on the two containers are quite similar over most of the container surface.

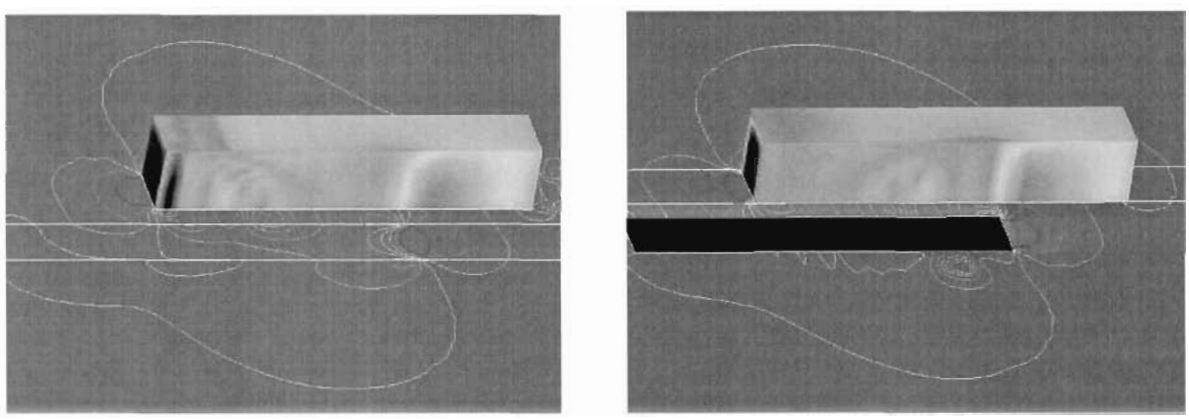

Figure B-1. Comparison of Surface Pressures for Fixed Container and Container Modeled Using Moving Boundary Condition (containers moving from right to left)

Pressure Contours Range from –0.15 psi (blue) to + 0.073 psi Pa (red)

A noticeable exception is the low-pressure (blue) region at the front-end of the container on its sides. This low-pressure is due to the flow separation at the corners of the container and the interaction with the passing container, which produces a strong vortex. This vortex is stronger at the front of the fixed mesh than the corresponding vortex at the moving boundary condition. This discrepancy is attributed to the better mesh resolution at the corners of the container in the fixed mesh. It is not economical to achieve comparable resolution using the moving boundary condition as this would require a very fine mesh throughout the region occupied. The differences in pressure distribution translate into small differences in the force resultants on the two containers as seen in Figure B-2. These differences are most significant for the lift on the upper surface of the container (Fz) and for the drag on the container (Fx). Drag reached a maximum value of 340 lbf (1500 N). These differences were attributed to the effects described above. The lateral loads (Fy), which are the most important in this study, have a larger overall magnitude and smaller absolute error. Finally, it is important to note that no absolute comparison has been made in this study with experiment or other validated calculations. It was not expected that the static drag on the container would be accurately modeled, as a turbulence model was not included for these calculations. Rather, it was only assumed that the fixed mesh would give an accurate representation of the dynamic lateral loads on the container that mostly affect consist dynamic response. These loads resulted from the broad pressure field around the opposing container, so this seems to be a reasonable assumption.

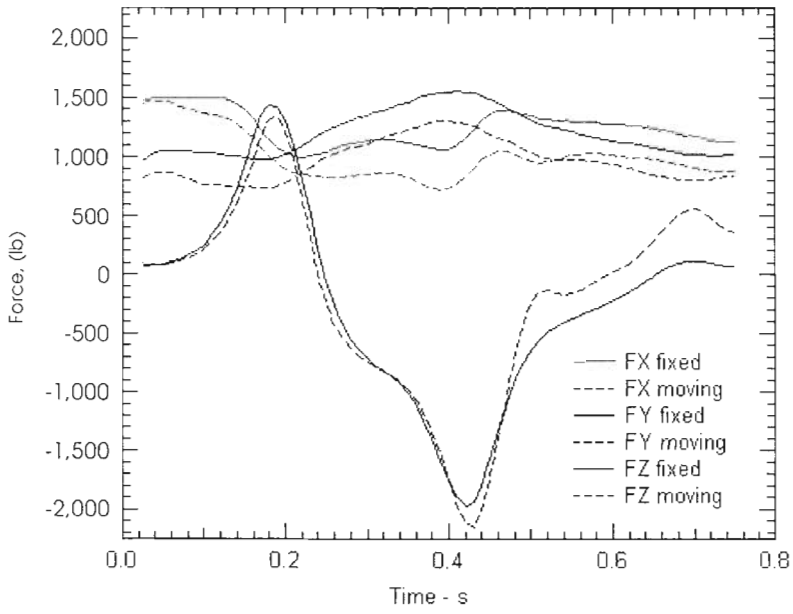

Figure B-2. Comparison of Force Resultants on Fixed Container with Those on the Moving Boundary Condition

APPENDIX-C

FORCE AND MOMENT RESULTANTS FOR CASES 1-15

This appendix summarizes the force and moment data in Cases 1-15. Table C-1 provides the parameters used in each run. The following pages show graphs of force and moment histories.

Table C-1. CFD Parameters for Cases 1-15

Case	Location[1]	Container Configuration		Train Velocity		Wind	
		Type[2]	Number[3]	Acela Express (mph)	Container (mph)	V_x (mph)	V_y (mph)
1	F	S	1	150	-50	0	0
2	F	S	3	150	-50	0	0
3	R	S	1	150	-50	0	0
4	F	C	1	150	-50	0	0
5	F	S	3	150	-50	-50	0
6	F	S	1	150	-50	50	0
7	F	S	1	150	50	50	0
8	F	S	1	150	50	-50	0
9	F	S	1	150	-50	0	-50
10	F	S	1	150	30	50	0
11	F	S	1	150	15	50	0
12	F	S	1	150	30	-50	0
13	F	S	1	150	15	-50	0
14	R	S	1	150	50	0	-50
15	F	S	1	120	50	-50	0

1. Refers to location of interaction – either at the front or at the back of Acela
2. Shape of container end, either simple (S) with a single or staggered edge.
3. Number of loaded container cars in a row.

Case 1

Single Container Passing Front of Acela Express
Velocities: Acela Express = +150 mph (67.07 m/s)
Container = -50 mph (-22.35 m/s)
Wind: Vx = 0.0; Vy = 0.0

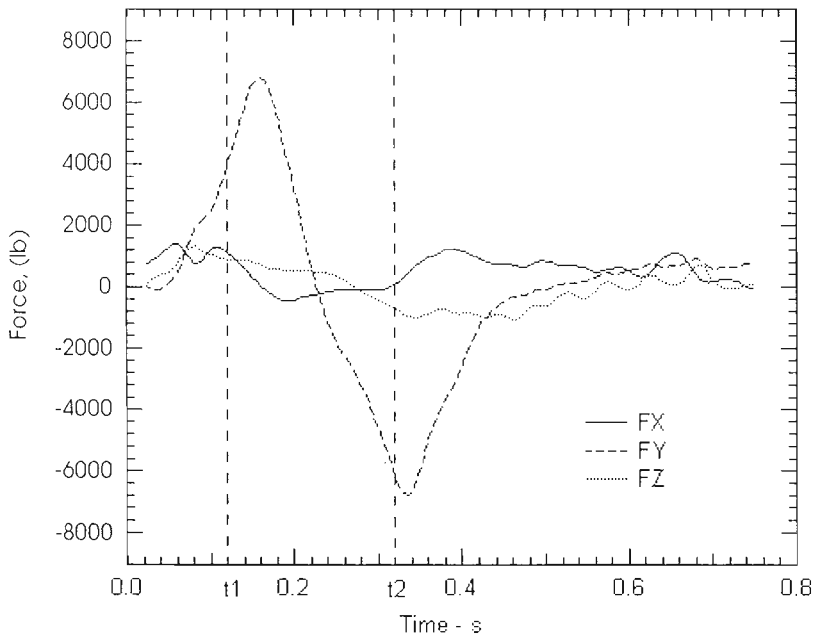

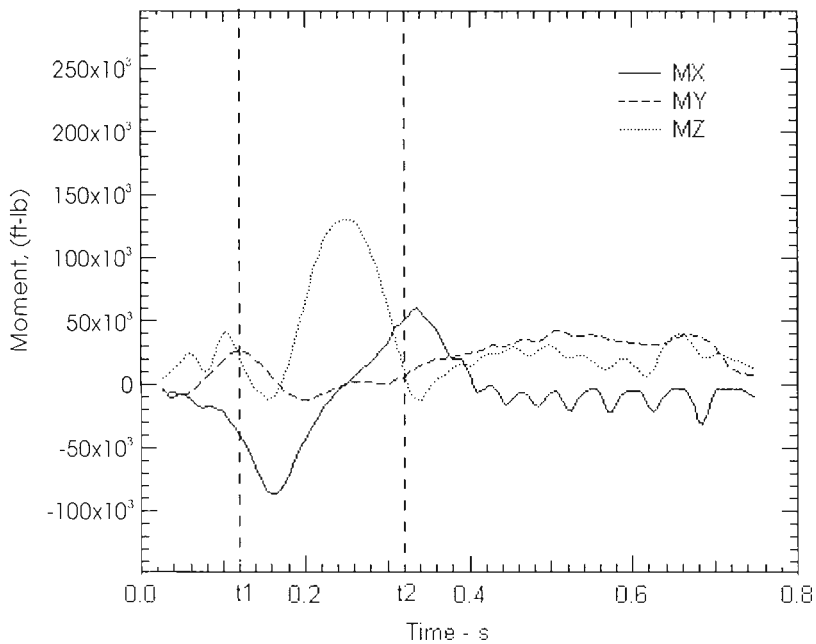

Case 2
Multiple (3) containers passing front of Acela Express; data given for center container
Velocities: **Acela Express = +150 mph (67.07 m/s)**
Container = -50 mph (-22.35 m/s)
Wind: Vx = 0.0; Vy = 0.

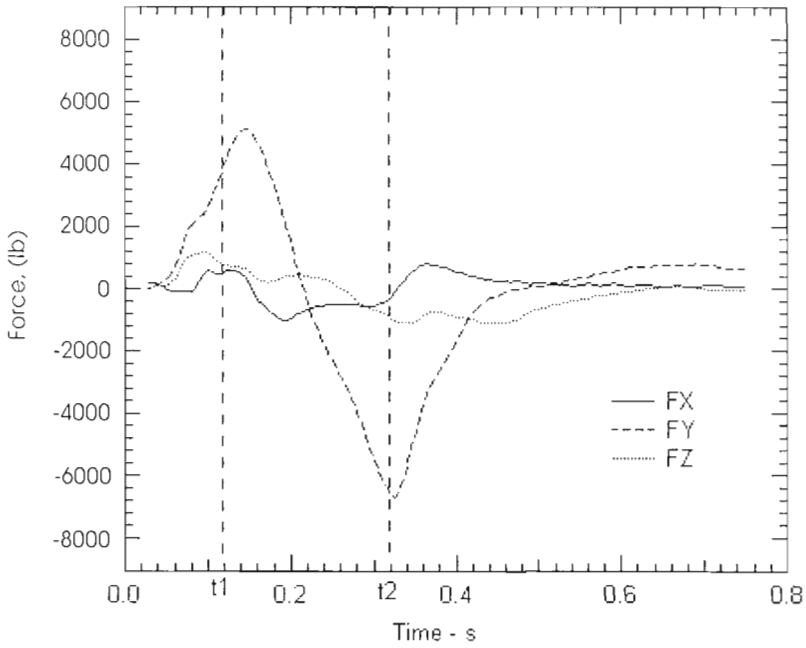

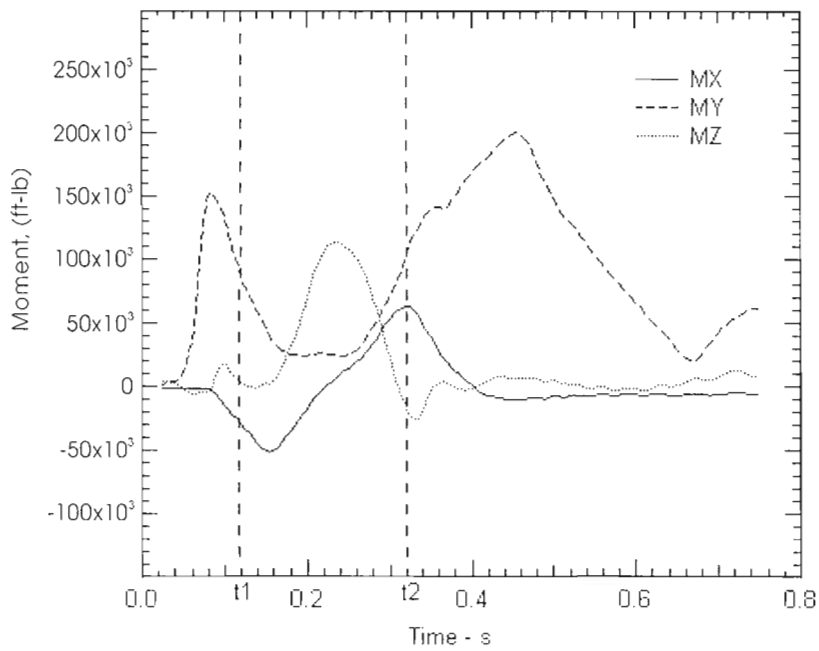

Case 4
Single container with staggered end passing front of Acela Express
Velocities: Acela Express = +150 mph (67.07 m/s)
Container = -50 mph (-22.35 m/s)
Wind: Vx = -50.0mph (-22.35 m/s); Vy = 0.0

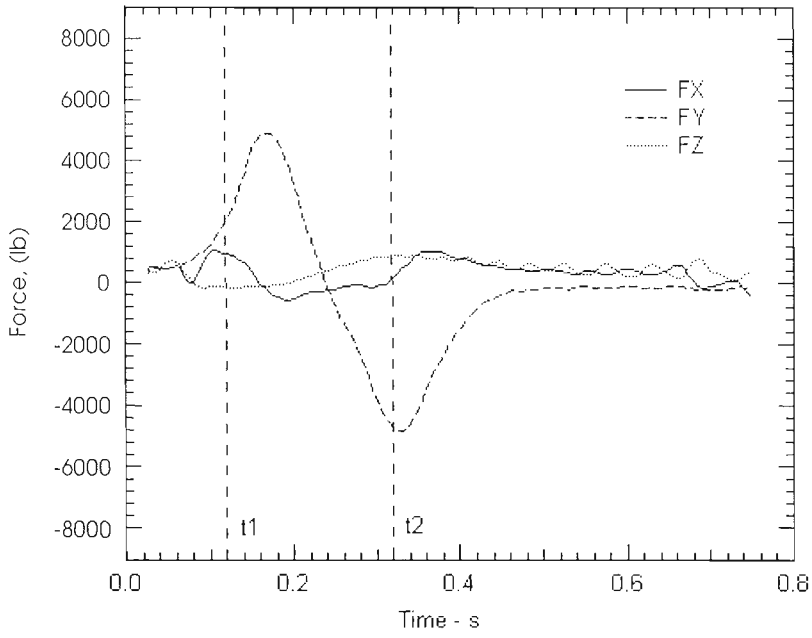

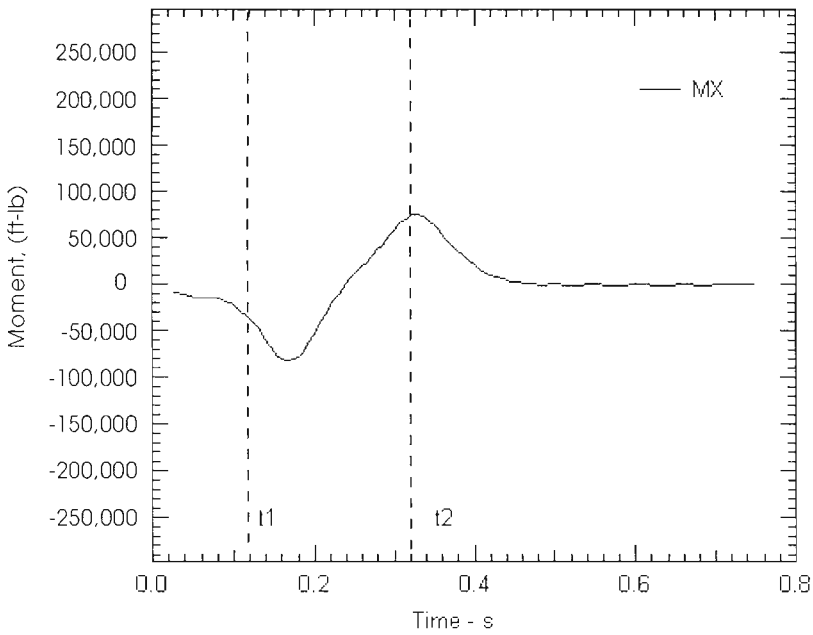

Case 5
Multiple (3) containers passing front of Acela Express; data given for center container
Velocities: Acela Express = +150 mph (67.07 m/s)
Container = -50 mph (-22.35 m/s)
Wind: Vx = -50.0mph (-22.35 m/s); Vy = 0.0

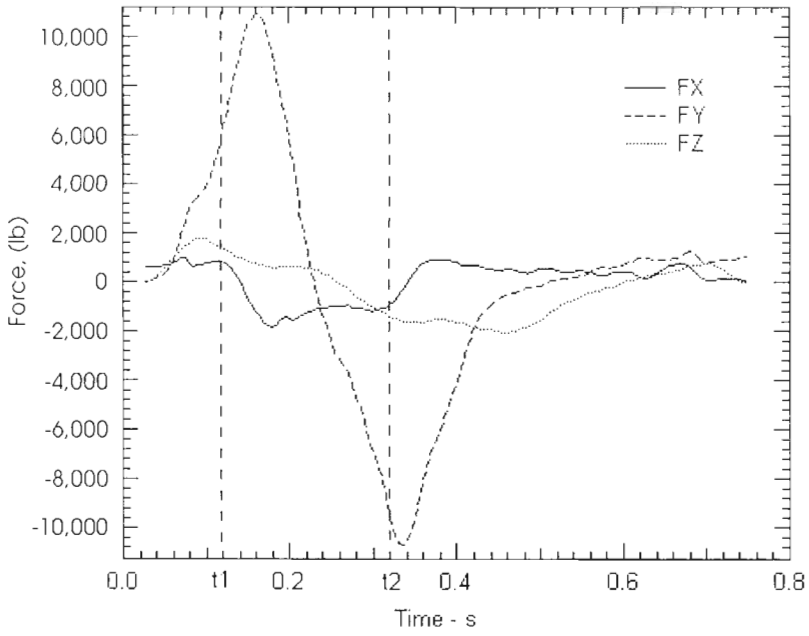

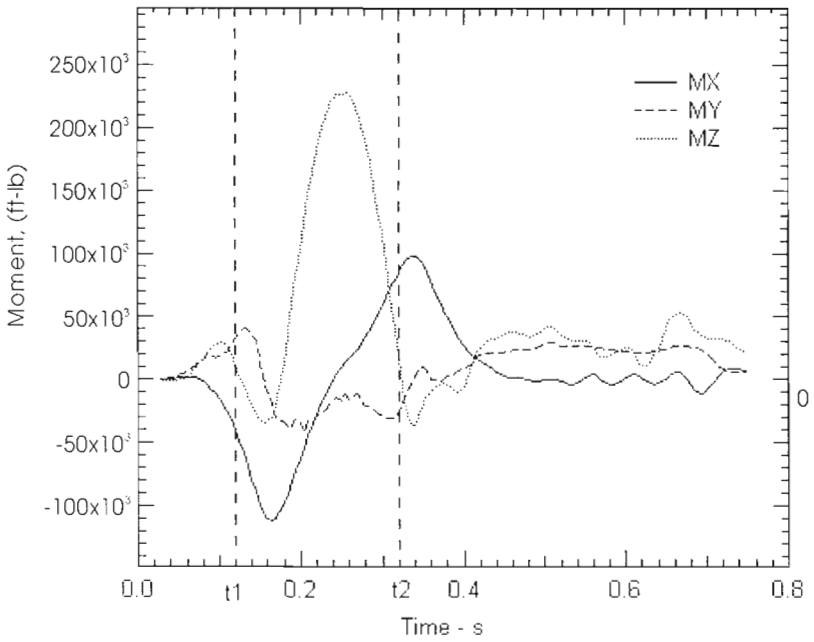

Case 6
Single container passing front of Acela Express
Velocities: Acela Express = +150 mph (67.07 m/s)
Container = -50 mph (22.35 m/s)
Wind: Vx = +50.0mph (22.35 m/s); Vy = 0.0

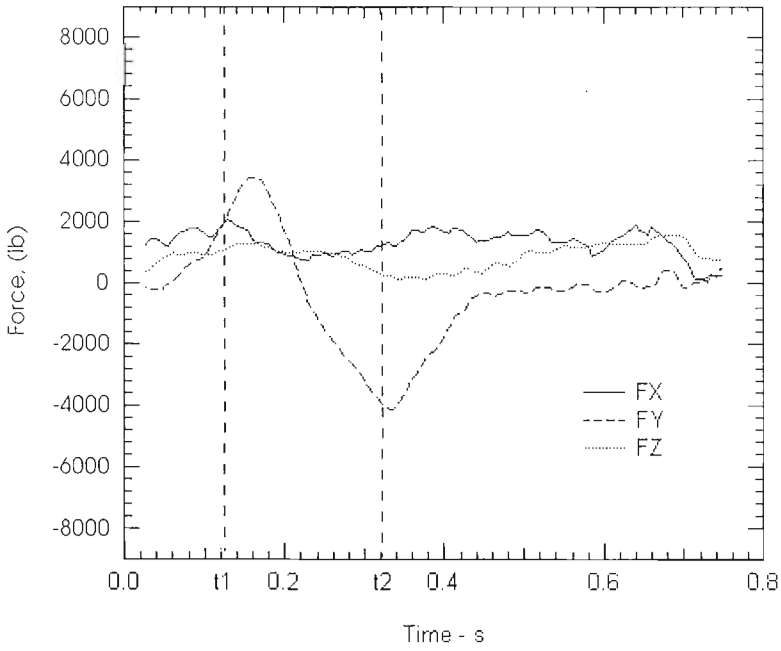

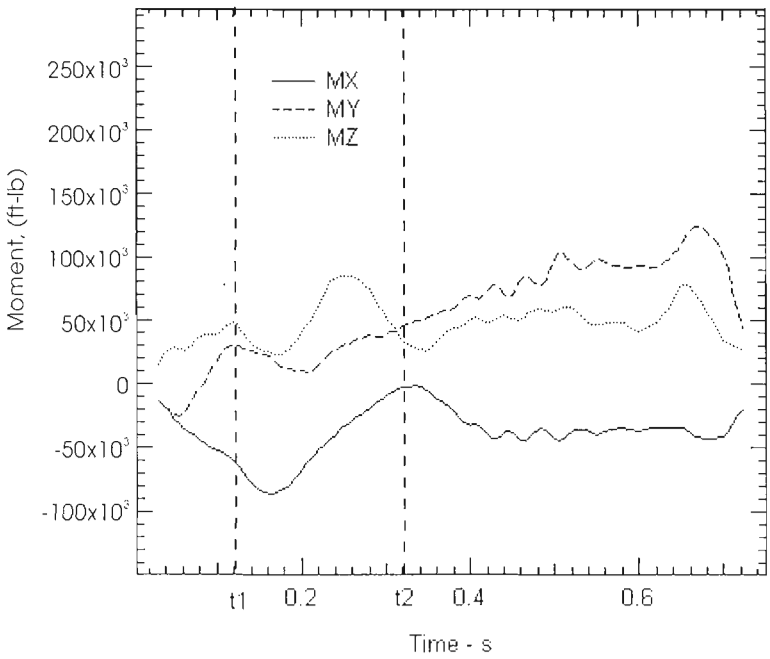

Case 7
Single container passing front of Acela Express
Velocities: **Acela Express = +150 mph (67.07 m/s)**
Container = +50 mph (22.35 m/s)
Wind: **Vx = +50.0mph (22.35 m/s); Vy = 0.0**

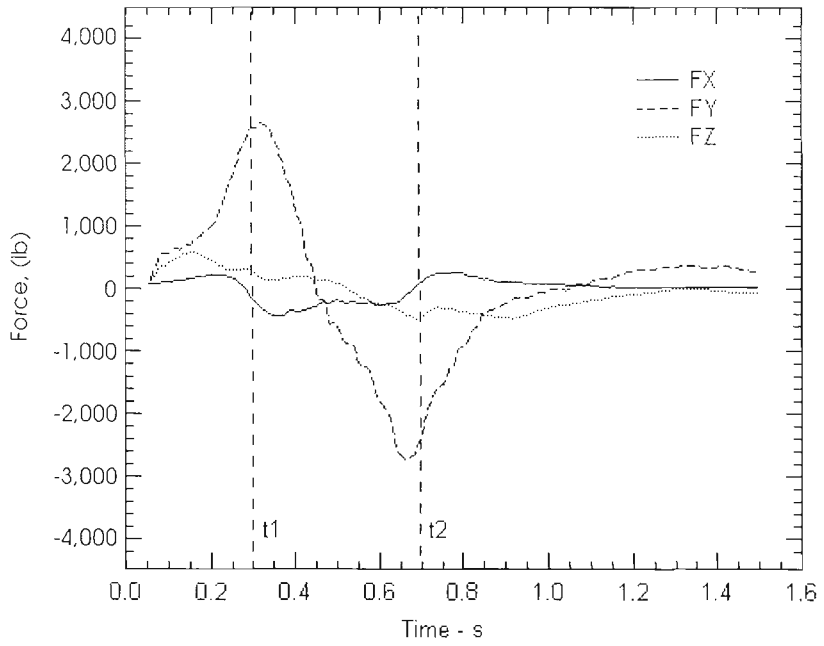

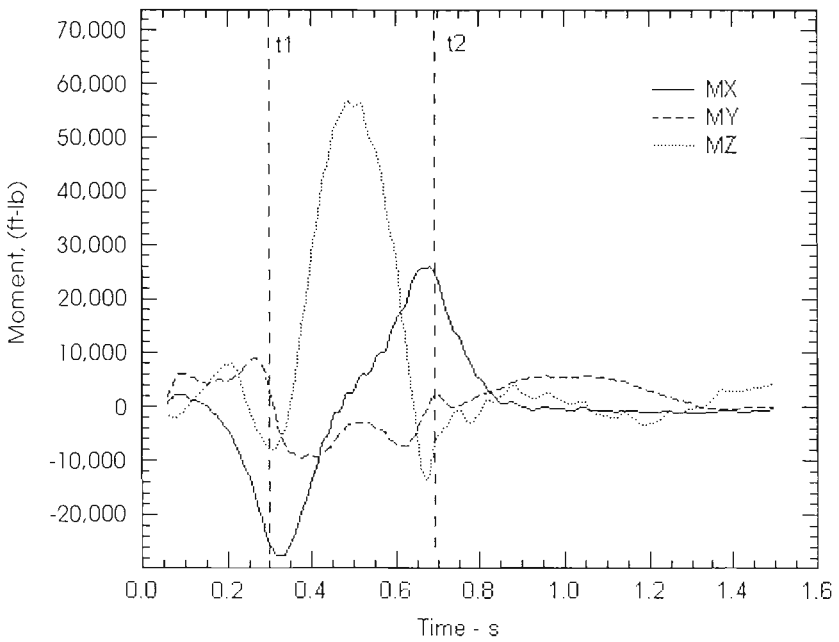

Case 8
Single container passing front of Acela Express
Velocities: **Acela Express = +150 mph (67.07 m/s)**
Container = +50 mph (22.35 m/s)
Wind: **Vx = -50.0mph (-22.35 m/s); Vy = 0.0**

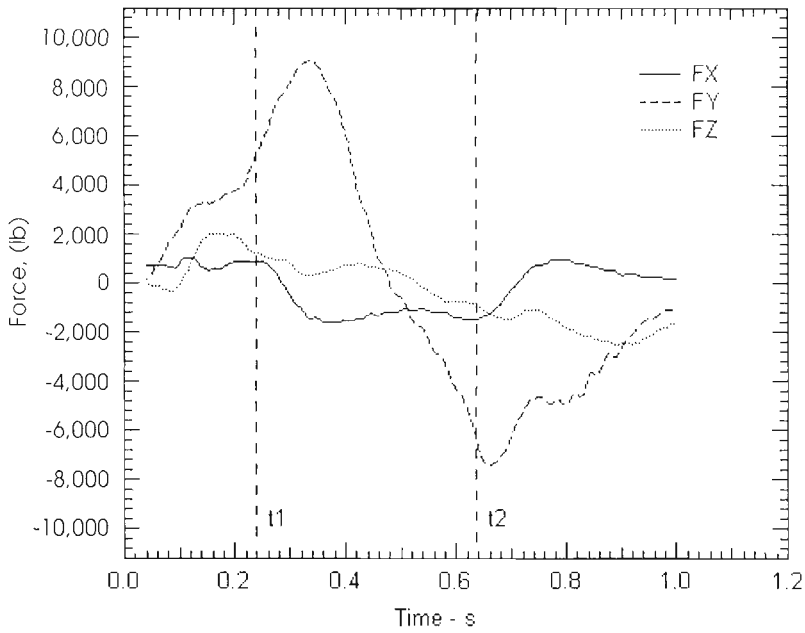

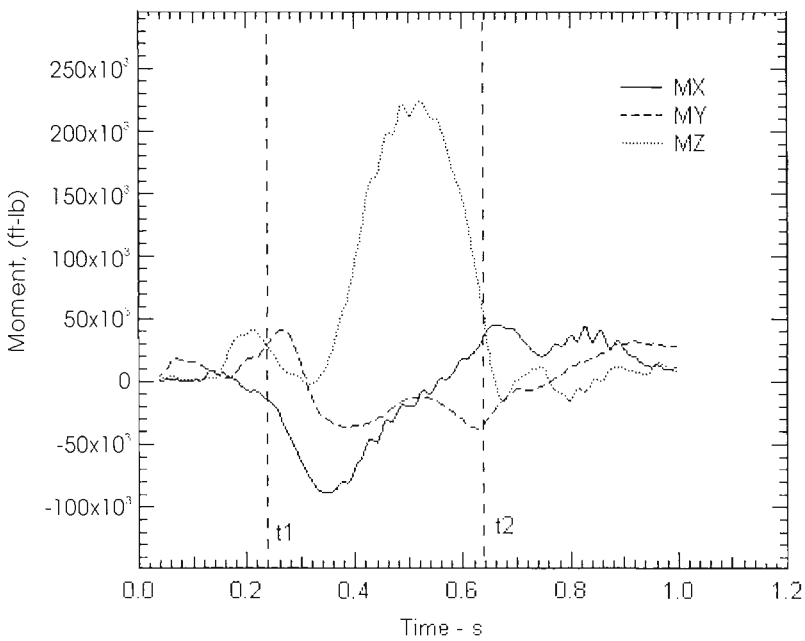

Case 9
Single container passing front of Acela Express
Velocities: **Acela Express = +150 mph (67.07 m/s)**
Container = -50 mph (22.35 m/s)
Wind: **Vx = 0.0mph ;Vy = -50.0 (-22.35 m/s)**

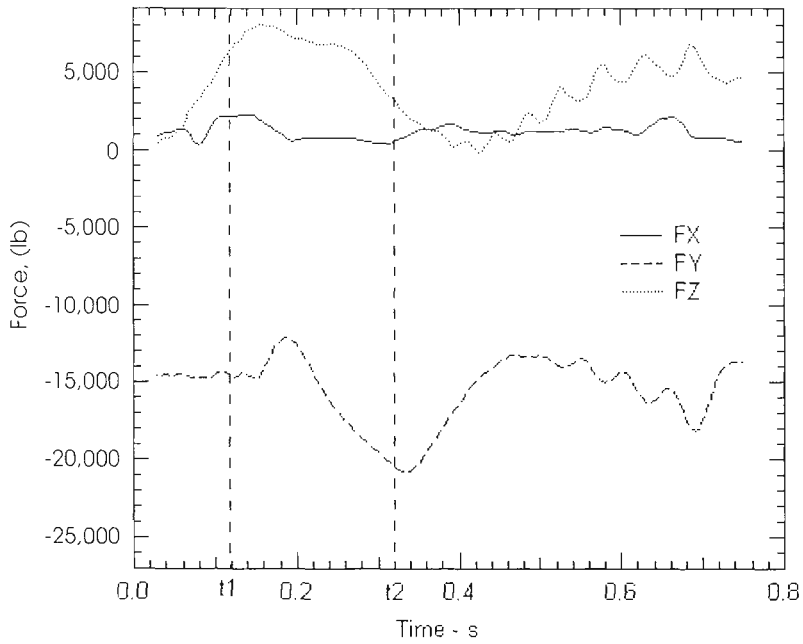

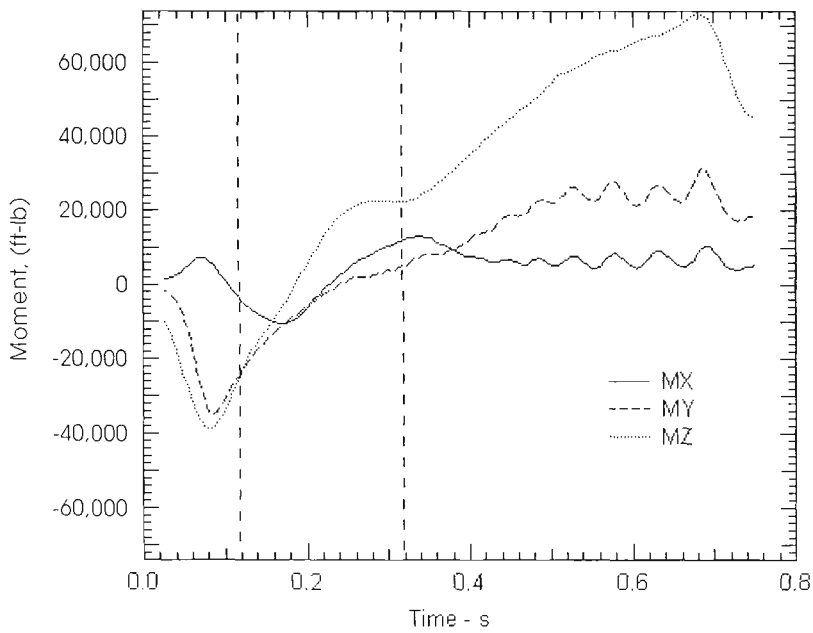

Case 10
Single container passing front of Acela Express
Velocities: **Acela Express = +150 mph (67.07 m/s)**
Container = +30 mph (13.41 m/s)
Wind: **Vx = +50.0mph (22.35 m/s); Vy = 0.0**

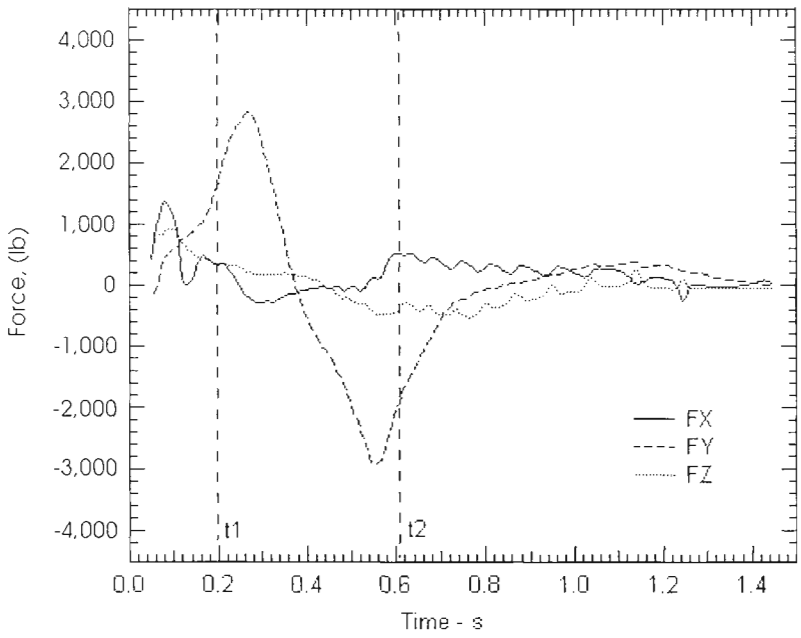

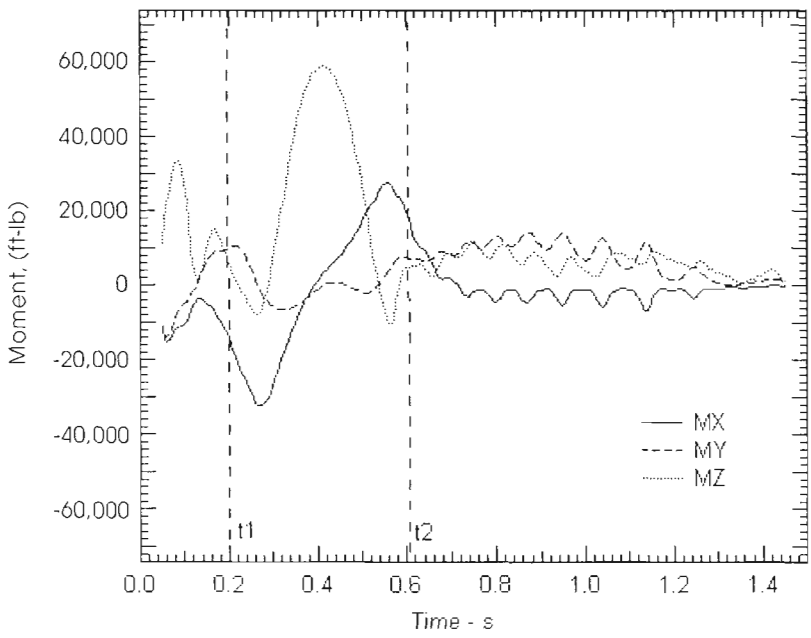

Case 11
Single container passing front of Acela Express
Velocities: **Acela Express = +150 mph (67.07 m/s)**
Container = +15 mph (6.7 m/s)
Wind: **Vx = +50.0mph (22.35 m/s); Vy = 0.0**

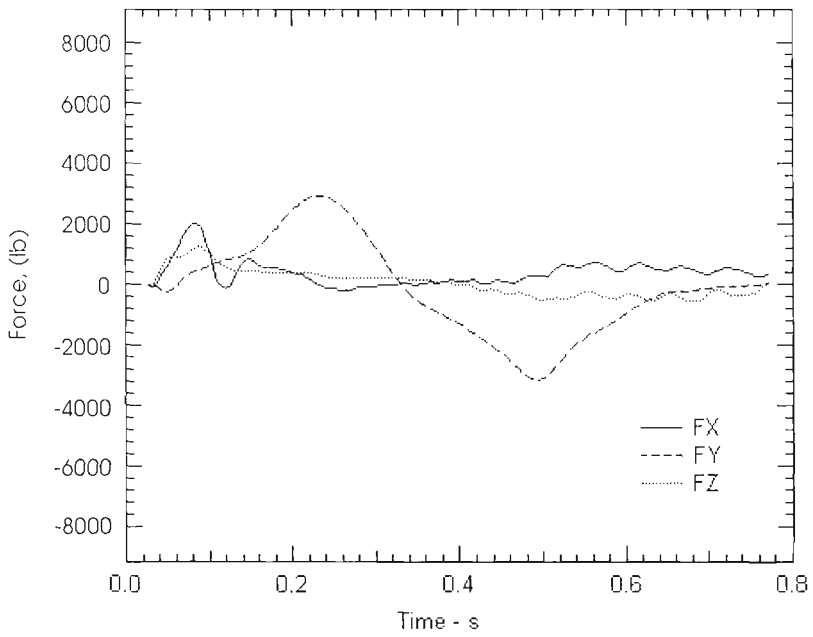

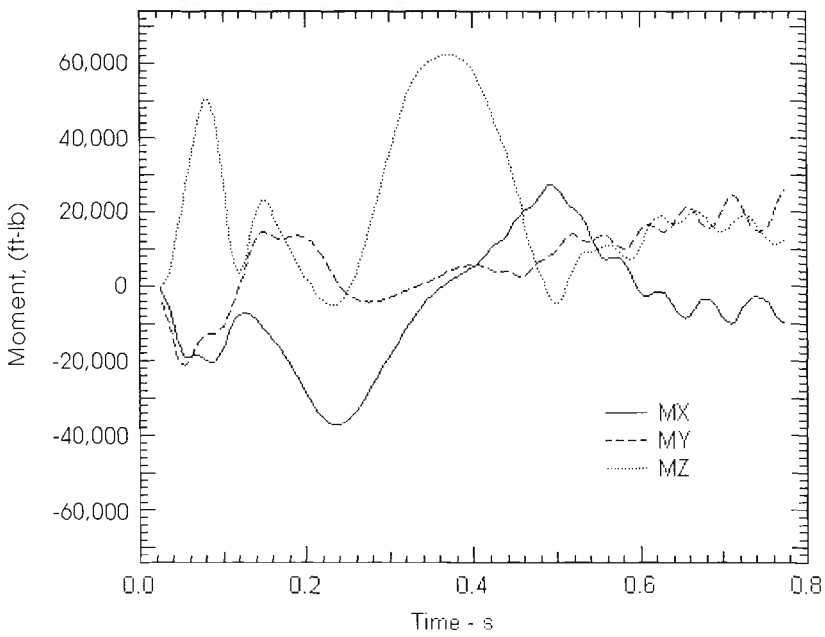

Case 12
Single container passing front of Acela Express
Velocities: **Acela Express = +150 mph (67.07 m/s)**
Container +30 mph (13.41 m/s)
Wind: **Vx = -50.0mph (-22.35 m/s); Vy = 0.0**

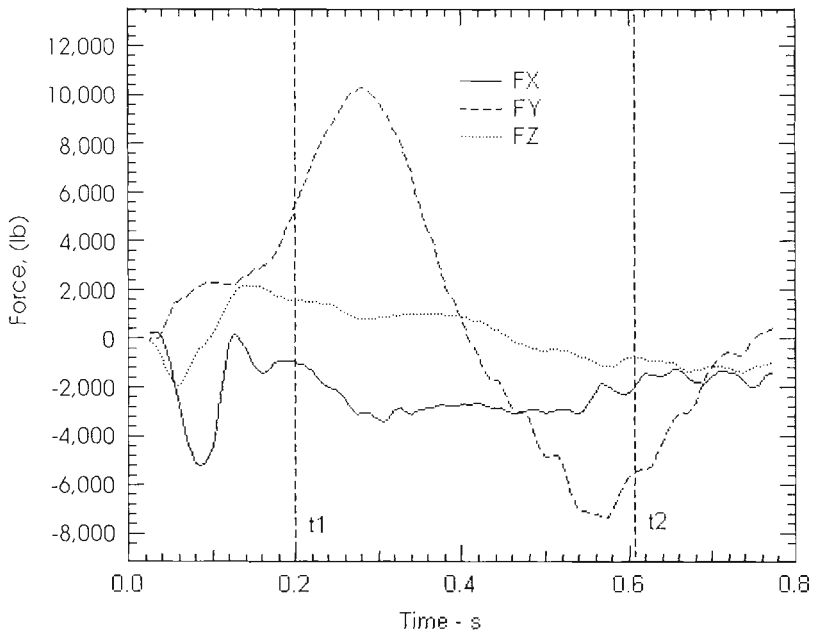

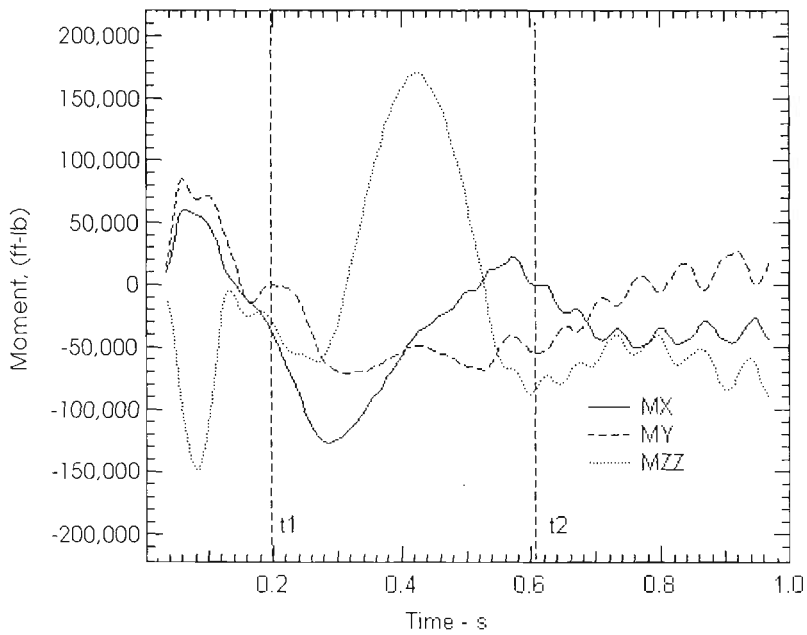

Case 13
Single container passing front of Acela Express
Velocities: **Acela Express = +150 mph (67.07 m/s)**
Container = +15 mph (6.7 m/s)
Wind: **Vx = -50.0mph (-22.35 m/s); Vy = 0.0**

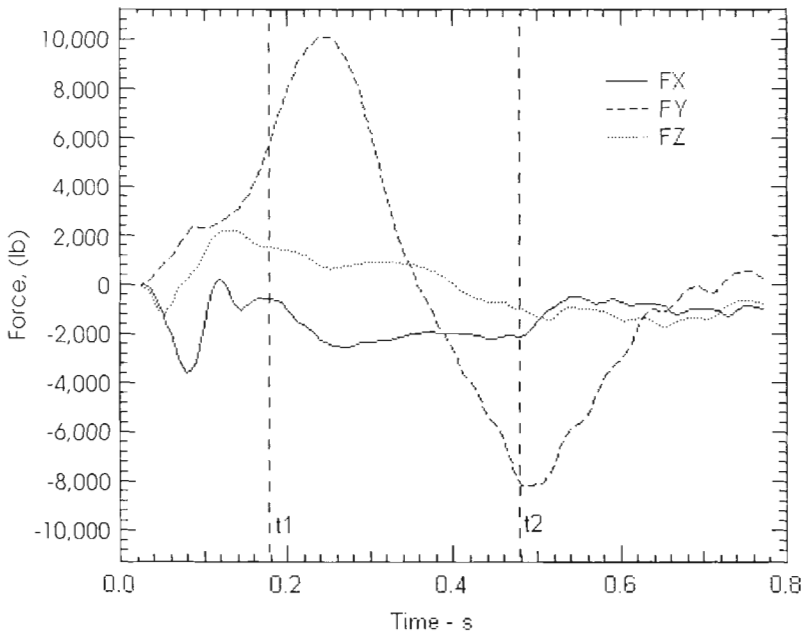

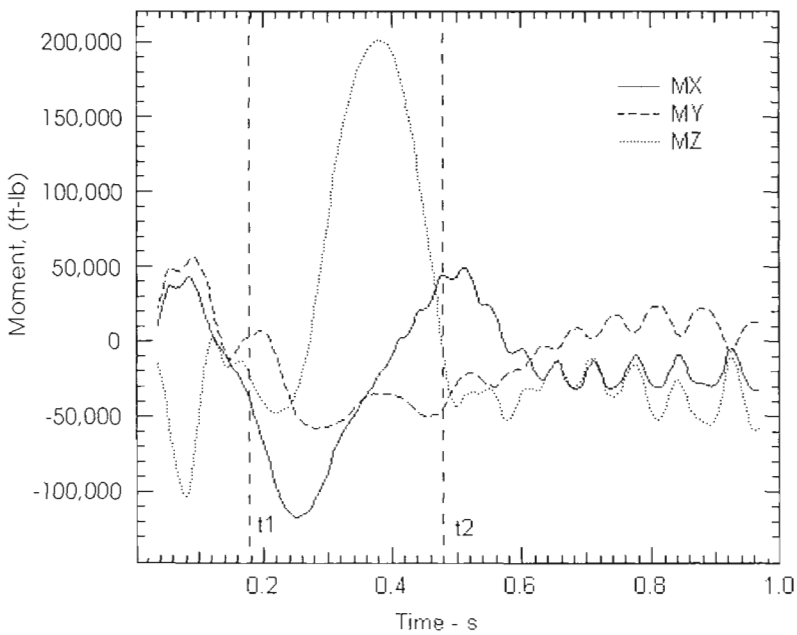

Case 14
Single container passing rear of Acela Express
Velocities: **Acela Express = +150 mph (67.07 m/s)**
Container = -50 mph (22.35 m/s)
Wind: **Vx = 0.0mph; Vy = -50.0 (-22.35 m/s)**

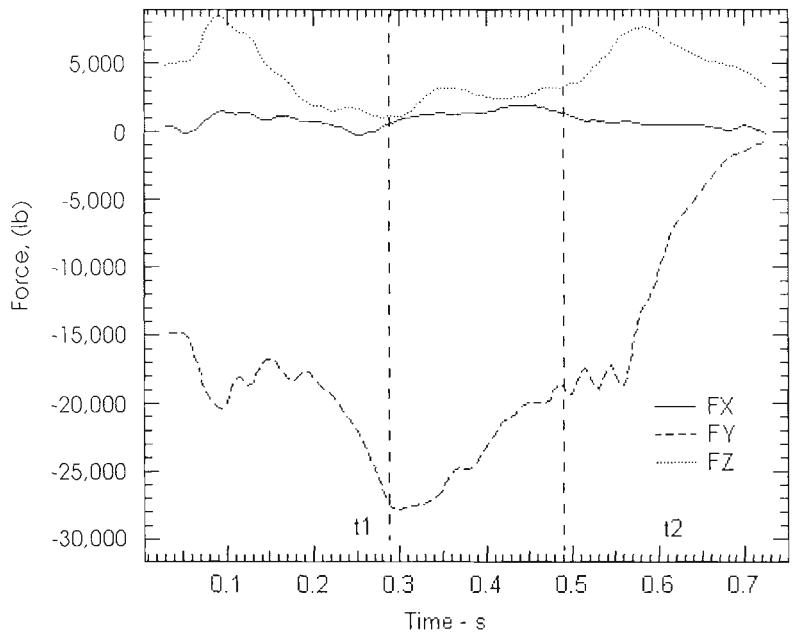

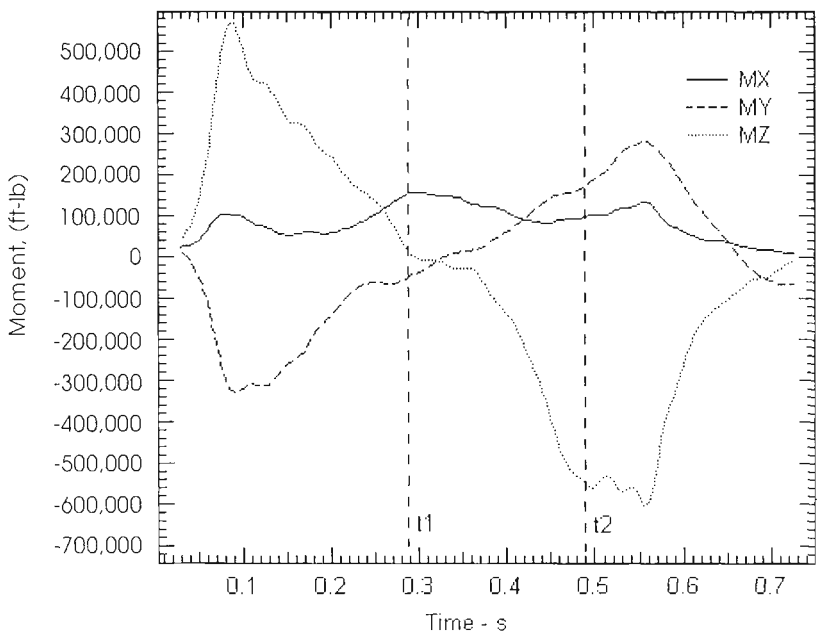

Case 15
Single container passing front of Acela Express
Velocities: Acela Express = +150 mph (67.07 m/s)
Container = -50 mph (22.35 m/s)
Wind: Vx = +50.0mph (22.35 m/s); Vy = 0.0

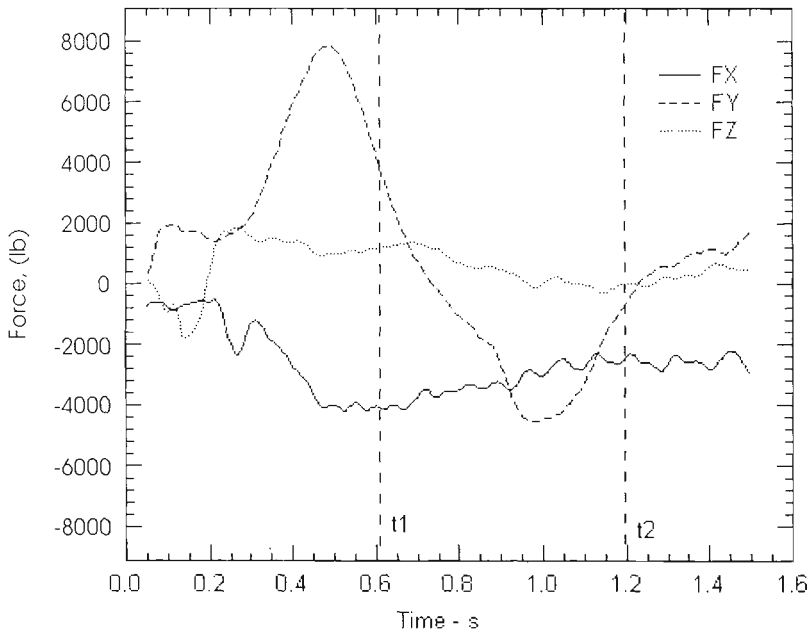

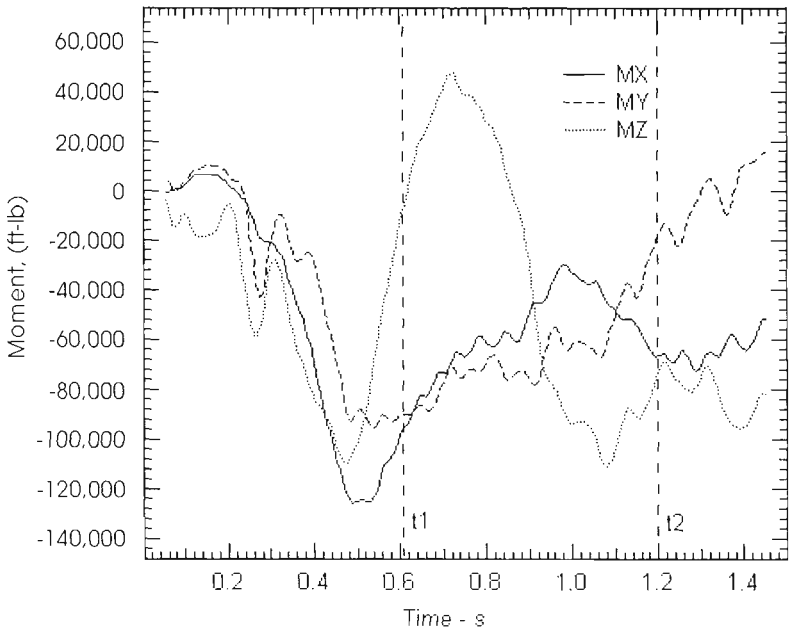

REFERENCES

1. Voss, G., and Wiebals, R., "Dynamic Pressure on Window Panes in Passenger Cars upon Meeting other Trains and Passing Through Tunnels." June, 1975. Translation supplied by John A. Volpe National Transportation Systems Center

2. Marchand, P., and Marmet, L. *Reviews of Scientific Instruments*. 54(8) 1034, 1983.